JOURNAL OF GEOPHYSICAL RESEARCH, VOL. 102, NO. D13, PAGES 15,849–15,866, JULY 20, 1997

Variations in the predicted spatial distribution of atmospheric nitrogen deposition and their impact on carbon uptake by terrestrial ecosystems

Elisabeth A. Holland,[1] B. H. Braswell,[2] Jean-François Lamarque,[1] Alan Townsend,[1,3] James Sulzman,[1] Jean-François Müller,[4] Frank Dentener,[5] Guy Brasseur,[1] H. Levy II,[6] Joyce E. Penner,[7] and Geert-Jan Roelofs[8]

Abstract. Widespread mobilization of nitrogen into the atmosphere from industry, agriculture, and biomass burning and its subsequent deposition have the potential to alleviate nitrogen limitation of productivity in terrestrial ecosystems, and may contribute to enhanced terrestrial carbon uptake. To evaluate the importance of the spatial distribution of nitrogen deposition for carbon uptake and to better quantify its magnitude and uncertainty NO_y-N deposition fields from five different three-dimensional chemical models, GCTM, GRANTOUR, IMAGES, MOGUNTIA, and ECHAM were used to drive NDEP, a perturbation model of terrestrial carbon uptake. Differences in atmospheric sources of NO_x-N, transport, resolution, and representation of chemistry, contribute to the distinct spatial patterns of nitrogen deposition on the global land surface; these differences lead to distinct patterns of carbon uptake that vary between 0.7 and 1.3 Gt C yr^{-1} globally. Less than 10% of the nitrogen was deposited on forests which were most able to respond with increased carbon storage because of the wide C:N ratio of wood as well as its long lifetime. Addition of NH_x-N to NO_y-N deposition, increased global terrestrial carbon storage to between 1.5 and 2.0 Gt C yr^{-1}, while the "missing terrestrial sink" is quite similar in magnitude. Thus global air pollution appears to be an important influence on the global carbon cycle. If N fertilization of the terrestrial biosphere accounts for the "missing" C sink or a substantial portion of it, we would expect significant reductions in its magnitude over the next century as terrestrial ecosystems become N saturated and O_3 pollution expands.

Introduction

It is becoming increasingly clear that human activities, including urbanization, industrialization, and the expansion and intensification of agriculture, affect the radiative balance, dynamics, and chemistry of the atmosphere through changes in the concentrations of trace constituents. Among these, carbon dioxide, nitric oxide, and more generally, the members of the NO_y and NH_x families ($NO_y = NO_x + HNO_2 + HNO_3 + HO_2NO_2 + NO_3 + N_2O_5 +$ PAN (peroxyacetyl nitrate); $NO_x = NO + NO_2$; $NH_x = NH_3 + NH_4^+$), play a major role. Far from being independent, NO_y and CO_2 are linked through the biosphere [*Vitousek*, 1994]. Release of nitrogen to the atmosphere influences the chemical reactivity of the troposphere, thus regulating the abundance of radiatively active gases including CH_4 and O_3, and, potentially, the productivity of the terrestrial biosphere through nitrogen deposition [*Logan*, 1981, 1983; *Peterson and Melillo*, 1985; *Schindler and Bayley*, 1993; *Hudson et al.*, 1994; *Galloway et al.*, 1995; *Schimel et al.*, 1995; *Schimel*, 1995].

In most terrestrial, as in some oceanic ecosystems, net primary production is limited by nitrogen availability; the exceptions are "N–saturated" temperate ecosystems and regions of the humid tropics which are limited by phosphorus [*Aber et al.*, 1989; *Schulze*, 1989; *McNulty and Aber*, 1993; *Vitousek*, 1994]. Thus, N constrains how much atmospheric CO_2 can be converted to organic carbon compounds via photosynthesis. Additional nitrogen deposited through precipitation or dry deposition can stimulate plant production, and thereby result in storage of atmospheric carbon dioxide. Resulting storage (which could persist for more than a few years) can be as either increased wood accumulation or storage in soil organic matter (SOM), as these are the only two ecosystem carbon compartments with turnover times generally longer than a decade [*Schimel et al.*, 1994; *Townsend et al.*, 1996]. Mole for mole, much more carbon is stored in wood than in SOM per unit nitrogen deposited, because the stoichiometric relationship of carbon to nitrogen for wood is 150-300:1 and for SOM it is 10-14:1. If, by contrast, the nitrogen is deposited on cultivated lands, the result is no or negligible carbon storage. Abundant annual crops have no perennial tissue in which to store the carbon and most cultivated lands already receive large inputs of nitrogen through fertilization. Therefore, the crops will not use the additional nitrogen provided through deposition to grow more plant tissue which would be stored as SOM. Furthermore, cultivated lands have been shown to lose large amounts of soil organic matter following the onset of cultivation

[1]NationalCenter for Atmospheric Research, Boulder, Colorado.
[2]University of New Hampshire, Durham.
[3]University of Colorado, Boulder.
[4]Belgian Institute for Space Aeronomy, Brussels.
[5]Department of Air Quality, Wageningen Agricultural University, Wageningen, The Netherlands.
[6]Geophysical Fluid Dynamics Laboratory, Princeton, New Jersey.
[7]Atmospheric, Oceanic, and Space Sciences, University of Michigan, Ann Arbor.
[8]Institute for Marine and Atmospheric Research Utrecht, Princetonplein, Utrecht, The Netherlands.

Paper number 96JD03164.
0148-0227/97/96JD-03164$09.00

[*Bauer and Black*, 1983; *Parton et al.*, 1987; *Esser*, 1990; *Davidson and Ackerman*, 1993]. The summary result is that carbon uptake from nitrogen deposition is determined by (1) the details of biogeochemical cycling, (2) spatial distributions of land and vegetation cover and (3) the aspect examined in this paper: the spatial distribution and quantity of nitrogen deposited.

Approach

The deposited nitrogen of interest in this study is that N derived from both industrialization and the expansion of metro-agro-plexes, essentially the additional N which represents a perturbation to the pre-industrial nitrogen cycle [*Chameides et al.*, 1994]. There is no globally distributed sampling of either wet or dry nitrogen deposition. Measurements of precipitation inputs of many cations and anions, including NH_4^+ and NO_3^-, have been made in country-by-country networks established to quantify acid precipitation, but these measurements provide partial coverage of the globe and often do not include all of the nitrogenous compounds deposited. Measurements of dry deposition are particularly sparse (U.S. Environmental Protection Agency) [*Edgerton et al.*, 1992]. Three-dimensional chemical transport models provide globally distributed information on the deposition of nitrogen, and allow the separation of nitrogen into that attributed to background processes and that to the intensification of human activity. Such information can then be used in a perturbation model. We use five such models to represent variations in the spatial distribution of the deposited nitrogen: ECHAM [*Roelofs and Lelieveld*, 1995]; GCTM [*Levy et al.*, 1996; H. Levy et al., Tropospheric NO_x: Its sources and distribution, submitted to *Journal of Geophysical Research*, 1996; hereinafter referred to as submitted paper]; GRANTOUR [*Penner et al.*, 1991, 1994]; IMAGES [*Müller*, 1992; *Müller and Brasseur*, 1995]; and MOGUNTIA [*Zimmermann*, 1988; *Zimmermann et al.*, 1989; *Dentener and Crutzen*, 1993, 1994]. The models differ in the source magnitudes and distributions of NO_x-N used, in their chemical transformation schemes, and in the way compounds are transported. A summary of the differences among the models is provided in Tables 1, 2 and 3 and are discussed below. All of the models include NO_x-N emissions, chemistry and transport. However, only one model, MOGUNTIA, represents NH_x-N emissions and their subsequent fate. Thus, model-to-model comparisons of NO_y-N deposition consider only the fate of emitted NO_x-N, which underestimates total N deposition by more than 50% [*Dentener and Crutzen*, 1994]. Our most comprehensive estimate of increased carbon storage from N deposition is made using both NH_x-N and NO_y-N deposition.

The influence of N deposition cannot be described by examining only the N that is deposited within a single year (as in previous estimates by *Peterson and Melillo* [1985], and *Schindler and Bayley* [1993]) because N is continually recycled in terrestrial ecosystems by the release or mineralization of N during decomposition and subsequent plant and microbial uptake of that N. Therefore, in the NDEP model, we calculate the cumulative effect of N deposition by estimating the amount deposited over the last century, beginning with 1860. The nitrogen and carbon fixed as a result of that deposition then cycles and the nitrogen is recirculated within the ecosystem allowing for losses due to leaching and gaseous emissions. All estimates of carbon storage are thus the cumulative result of nitrogen deposition and differ substantially from other "instantaneous" estimates [*Peterson and Melillo*, 1985; *Schindler and Bayley*, 1993].

Terrestrial Model Description

Carbon and nitrogen pools in the NDEP perturbation model are those due to nitrogen deposition only, and therefore were set initially to zero. Changes in woody and nonwoody carbon pools (C_w ,C_{nw}) depend on the flux of available nitrogen (N_{av}), an allocation term (f_w) which specifies the fraction of C going to woody biomass, the C:N ratio of each pool, and the residence time of carbon in the pools:

$$\frac{dC_w}{dt} = f_w \bullet CN_w \bullet N_{av} - \alpha_w \bullet C_w \quad (1)$$

$$\frac{dC_{nw}}{dt} = (1 - f_w) \bullet CN_{nw} \bullet N_{av} - \alpha_{nw} \bullet C_{nw} \quad (2)$$

where α_w and α_{nw} represent yearly litter fall fractions from woody and nonwoody vegetation, respectively, and are equal to the inverse of the residence time. Litter fall from each pool enters the detrital C pool (C_d), which changes according to

$$\frac{dC_d}{dt} = \alpha_w \bullet C_w + \alpha_{nw} \bullet C_{nw} - (\alpha_{da} + \alpha_{dm} + \alpha_{ds}) \bullet C_d \quad (3)$$

where α_{dm}, α_{ds}, and α_{da} are transfer coefficients from the detrital pool to the microbial pool, the slow pool, and the atmosphere (respiration). The slow pool is the applied to the pool of soil organic carbon and nitrogen which has decadal to centennial turnover times depending on the local climate [*Parton et al.*, 1993]. The values depend on lignin content and mean annual temperature, and are taken from a global analysis of soil organic matter turnover times [*Schimel et al.*, 1994]. Changes in microbial (C_m) and slow (C_s) carbon pools are calculated from

$$\frac{dC_m}{dt} = \alpha_{dm} \bullet C_d - (\alpha_{ma} + \alpha_{ms}) \bullet C_m \quad (4)$$

$$\frac{dC_s}{dt} = \alpha_{ds} \bullet C_d + \alpha_{ms} \bullet C_m - \alpha_{ma} \bullet C_s \quad (5)$$

where again the values are from *Schimel et al.* [1994].

Changes in woody (N_w), nonwoody (N_{nw}), microbial (N_m), and slow (N_s) nitrogen pools are the same as those for carbon, divided by the C:N ratios of the pool:

$$\frac{dN_i}{dt} = \frac{dC_i / dt}{CN_i} \quad (6)$$

but changes in detrital nitrogen (N_d) depend on the C:N ratios of both vegetation and detrital pools:

$$\frac{dN_d}{dt} = \frac{(\alpha_w \bullet C_w)}{CN_w} + \frac{(\alpha_{nw} \bullet C_{nw})}{CN_{nw}} - \frac{(\alpha_{da} + \alpha_{dm} + \alpha_{ds}) \bullet C_d}{CN_d} \quad (7)$$

Net nitrogen mineralization (N_{min}) depends on the carbon transfer and the C:N ratios of all three soil pools. Enough N to satisfy the C:N ratio of each pool is "immobilized" during each transfer, with the remainder contributing to N_{min}:

$$N_{min} = \left[\frac{(\alpha_{da} + \alpha_{dm} + \alpha_{ds}) \bullet C_d}{CN_d} + \frac{(\alpha_{ma} + \alpha_{ms}) \bullet C_m}{CN_m} + \frac{\alpha_{sa} \bullet C_s}{CN_s} \right] - \left[\frac{\alpha_{dm} \bullet C_d}{CN_m} + \frac{\alpha_{ds} \bullet C_d}{CN_s} + \frac{\alpha_{ms} \bullet C_m}{CN_s} \right] \quad (8)$$

and available nitrogen for plant uptake (N_{av}) is then calculated as the current year's deposition plus net N mineralization minus the rate of N loss (20% of N_{av}):

$$N_{av} = N_{dep} + N_{min} - N_{loss} \quad (9)$$

The proportion of N lost from an ecosystem was set at 20% for most of the simulations; this value is an approximate mean from a number of nitrogen budget studies in temperate systems [*Likens et al.*, 1981; *Johnson et al.*, 1988]. The sensitivity to variations in N_{loss} was discussed by *Townsend et al.* [1996] and is discussed further in the following sections.

Finally, the total carbon sink due to N deposition at any time t is equal to the sum of the changes in each of the five carbon pools:

$$\frac{dC_{sink}}{dt} = \frac{d(C_w + C_{nw} + C_d + C_m + C_s)}{dt} \quad (10)$$

Description and Comparison of Three-Dimensional Chemical Transport Models

All of the models included in the study incorporate the same basic elements: sources of NO_x-N (or NH_x-N) are released on a latitude by longitude grid and transported. The compounds undergo chemical transformation, are deposited back to the surface, or are released to the stratosphere. Surface emissions of nitrous oxide (N_2O), the largest source of surface emitted N to the stratosphere, is not included in the models used here. The primary mechanisms for NO_x-N and NO_y-N removal are by chemical transformation, precipitation and dry deposition. The details of how the processes are represented, the space and time resolution used, and the emphasis placed on different components differ substantially amongst the models. These differences are summarized in Table 1.

The spatial and temporal resolutions of the five different models differ from one another. GCTM has the finest spatial resolution with 2.4° by 2.4° grid cells and MOGUNTIA has the coarsest resolution with 10° by 10° grids with ECHAM v. 3.2, GRANTOUR, and IMAGES falling somewhere in between the two. The height of the atmosphere represented varies between ~16 and 32 km, and the number of layers in the modeled atmosphere varies between 10 and 25 (Table 1). IMAGES uses the most finely resolved vertical layering, and MOGUNTIA the coarsest. Each model is elaborate in a different aspect: IMAGES has the most complex chemistry, while GCTM has the most refined spatial and temporal resolution.

The transport schemes used by the various models differ in the climatologies used to drive them and in the transport schemes. ECHAM is a general circulation model implemented such that chemistry and transport are interactive. The transport time step of the models ranges from 26 min for GCTM to 1 day for IMAGES. Two of the models, GCTM and GRANTOUR, use wind and precipitation fields generated by general circulation models. Two of the models, IMAGES and MOGUNTIA, used global climatologies of wind and precipitation. All of the models represent diffusion. They differ in the amount of subgrid mixing, the convective schemes used, and exchanges with the planetary boundary layer. ECHAM has the most sophisticated convective scheme with penetrative, shallow, and midlevel convection.

The complexity of the chemical schemes used differed among the five models. IMAGES used the most sophisticated chemistry with 125 reactions (including 26 photolytic reactions), 41 species including seven different hydrocarbons, oxygenated organics, PAN, MPAN, and N_2O_5 reactions on aerosols. GRANTOUR used a simple chemical scheme including HNO_3, NO, and NO_2 but no PAN or reactions with other organic species.

The spatial distribution of the deposited nitrogen depends on interactions of the transport and chemical schemes with both wet and dry deposition. Two of the models, ECHAM and GCTM, use the same dry deposition scheme, which includes effective wind speed. The other three models use essentially the following equation for dry deposition:

$$F = V_d n Y \quad (11)$$

where V_d is the deposition velocity, n is molecules cm^{-3}, and Y is the mixing ratio of the gas. Each model differed in the assigned deposition velocities and whether or not diurnal variations in deposition velocities were included. Comparisons of dry deposition velocities are provided in Table 2. Wet deposition depended on the rate of precipitation, but the details of the formulations varied, particularly the different types of precipitation represented and the solubility coefficients implemented for the different chemical species. Dry deposition velocities for NO_2 are consistent amongst the models but vary substantially for NO and HNO_3. Dry deposition velocities over land are specific to vegetation type for IMAGES but independent of vegetation type for the other models.

We used IMAGES, the locally available model, to perform detailed model analyses: we examined the influence of individual sources on N deposition, verified simulated wet deposition fluxes, and examined the correspondence between NO_y-N deposition and surface O_3 concentrations. The impacts of ambient O_3 and N deposition upon carbon storage in polluted areas are discussed in a following section.

Sources of NO_x

Total NO_x-N sources for the five models range from 35 to 48.8 Tg N yr^{-1} (Table 3). Variations in fossil fuel emissions were smaller (approximately 10%) and primarily driven by the choice of reference year. The lowest fossil fuel emissions were from GCTM, which used a reference year of 1985 [*Benkovitz et al.*, 1996]; GRANTOUR, which had the highest emissions, used 1990 as the reference year. The remainder of the variation amongst the NO_x-N emission estimates were driven by differences among the natural sources: lightning, biomass burning, and soils. The variability in the soil and part of the biomass burning sources are largely due to differing representations of biological controls over production, particularly the inclusion of canopy scavenging of NO_x-N emitted at the soil surface (see below). Transport and oxidation of N_2O from the stratosphere (0.2 to 0.64 Tg N yr^{-1}) and aircraft emissions (0.23 to 0.89 Tg N yr^{-1}) were small proportional contributions to the total budget. While the estimates of lightning production vary widely, lightning production of NO_x-N is

Table 1. Comparison of the Five Three-Dimensional Chemical Transport Models Used to Estimate N Deposition

	ECHAM[a]	GCTM[b]
	Spatial and Temporal Features	
Horizontal resolution	5.6°× 5.6°	2.4° × 2.4°
Vertical resolution	19 layers; surface to ~31.5 km	11 layers; 0.08 to ~31.4 km
Time resolution	40 min	26 min; calculations for 1 full cycle with no diurnal cycle or interannual variability
Scheme	Semi-Lagrangian advection	
Important features	Penetrative, shallow, and midlevel convection; convection includes up and down drafts; includes convective clouds	Horizontal second-order advection; fourth-order vertical mixing occurs with convectively unstable atmosphere (moist and dry); shear dependent vertical diffusion in bottom three layers to enhance PBL[f] mixing
Driven by	ECHAM GCM v.3.2	GFDL GCM
Variables calculated in GCM and used in CTM	Wind, precipitation; water vapor, radiation, large scale and convective cloud formation; boundary layer mixing	6-hour average; winds, total precipitation and dry and moist vertical stability
	On-line	Off-line
Transported species	O_3, CO, CH_4, HNO_3, H_2O_2, CH_3O_2H NO_y (NO, NO_2, NO_3, N_2O_5, HNO_4)	(HNO_3 + NO_3^-), (NO_x + N_2O_5), PAN,[g] PAC[h]
Photochemistry	CH_4-CO-NO_x-HO_x[k] + N_2O_5 on aerosols → HNO_3	CH_4-CO-NO_x-HO_x including PAN and limited NMHCs[l] (see prescribed fields); NO_x, NO_3 + N_2O_5 reactions on aerosols (according to *Dentener and Crutzen* [1993])
Prescribed fields	CH_4 surface concentrations	CH_4-CO-NO_x-HO_x, PAN + NHMCs calculated as monthly averages in two dimensions for gas phase. N_2O_5 heterogeneous dark chemistry calculated as monthly averages in three dimensions. Total column ozone
Dry	see GCTM	$\frac{\partial}{\partial t} R_{11}(i)\ \text{dry} = \frac{vd(i)}{\Delta Z}\left\{\left(R_{11}(i)\right)\frac{1}{\left[1 - v_d(i)/c_d\left\|\bar{v}_{eff}\right\|\right]}\right\}$ $R_{11}(i)$ mixing ratio for species 1 in lowest model level; $v_d(i)$ deposition velocity; ΔZ thickness of lowest model layer; $\left\|\bar{v}_{eff}\right\|$ model's effective wind speed; C_d globally averaged surface drag coefficient (0.002)
Species dry deposited	O_3, NO, NO_2, N_2O_5, HNO_3, H_2O_2	
Wet	$W_{surf} = \sum_{k=1,19} W(K) = \sum_{k=1,19} W_{pr}(K) + W_{ev}(K) + W_{bc}(K)$ W_{surf} wet deposition of soluble gases at surface; $W(K)$ wet deposition for individual model levels; $W_{pr}(K)$ in-cloud precipitation, larg- scale and convective clouds; $W_{ev}(K)$ evaporation of rain; $W_{bc}(K)$ below cloud scavenging	$W(K) = \frac{-FR}{Dt}$ W wet deposition flux of soluble gas from level (K); R tracer mixing ratio $F = \frac{Q\Delta + \rho}{LH}$ L liquid H_2O content; Q precipitation rate averaged over column cross-sectional area; ρ density of liquid H_2O; H column height and height considered is dependent on Richardson's number (R_{in}) for convective precipitating clouds: (R_{in} < 0.25 at 315 and 500 mbar levels); $L = 0.5 \times 10^{-6}$ g cm^{-3}; for nonconvective precipitating clouds, (R_{in} > 0.25 at 315 and 500 mbar levels); $L = 2 \times 10^{-6}$ g cm^{-3} for all other cases
Species subject to precipitation scavenging	HNO_3, H_2O_2, CH_2O, CH_3O_2H, HNO_4	HNO_3

[a] *Roelofs and Lelieveld* [1995].
[b] *Kasibhatla et al.* [1991, 1993], *Moxim et al.* [1996], *Levy et al* [1996, submitted paper, 1996].
[c] *Penner et al.* [1991, 1994].
[d] *Muller* [1992], *Müller and Brasseur* [1995], J.-F. Lamarque (personal communication, 1995)
[e] *Dentener and Crutzen* [1993].
[f] Planetary boundary layer.
[g] Peroxyacetic nitric anhydride
[h] Peroxyacetyl radical.

GRANTOUR[c]	IMAGES[d]	MOGUNTIA[e]
	Spatial and Temporal Features	
≈ 4.5° × 7.5°	5° × 5°	10° × 10°
12 layers; 0.09 to ~33.4 km	25 layers; 0.04 to ~22.5 km	10 layers; surface to ~16 km
6 hours; annual cycle; diurnal average with averaging coefficients from LLNL 2-D model	1 day except during first 3 days of the month, which have full diurnal cycle	2 hours
Transport		
Lagrangian advection	Semi-Lagrangian advection	
Vertical mixing by moist convection; interparcel mixing with shear dependent eddy diffusion; fixed large-scale diffusion coefficients	Deep convection; diffusion; subgrid mixing via turbulent mixing in PBL[f] and convective cloud formation	Deep cumulus convection; eddy diffusion based on standard deviation from the mean
LLNL CCM1 (from NCAR)	ECMWF mean winds (1985–1989) [*Trenberth and Olson*, 1988a, b]; precipitation from climatology of *Shea* [1986]; cumulonimbus and nimbostratus according to ISCCP	Monthly average winds [*Oort*, 1983]; precipitation climatology from *Jeager* [1976]; monthly average temperature [*Oort*, 1983]
Wind, precipitation, convective mass flux	N/A	N/A
Chemistry		
Off-line		
HNO_3, NO, NO_2, O_3, H_2O_2, NO_3, N_2O_5, CH_2O, CH_3OOH, HONO; CO + CH_4 fixed	O_3, NO_x, HNO_3, CO, CH_4, ethane, propane, isoprene, α-pinene, ethylene, propylene, OTHC,[i] CH_2O, PAN, MPAN,[j] CH_3OOH, C_2H_5OOH, C_3H_6OHOOH, CH_3COOOH	NO_x, HNO_3, O_3, $(NH_4)SO_4$, CO, CH_4, H_2O_2, H, SO_4, NH_3, NH_4^+, CH_2O, CH_3O, H, $CH_4H_2O_2$, DMS, SO_2, C_2-C_3-PAN-PPN
$NO_y \rightarrow HNO_3$	CH_4-CO-NO_x-HO_x + isoprene, C_2H_6, C_3H_6 + oxygenated organics;125 reactions with 26 photolytic reactions; N_2O_5 reaction on aerosols	CH_4-CO-NO_x-HO_x
NO + NO_2; photostationary states; no PAN or NMHCs in this version; N_2O_5 *rxn* on aerosols set to average value		N_2O_5, NO_2 + NO_y reaction on aerosols; photochemistry and sulfur/NH_x chemistry integrated
CO, CH_4 prescribed based on observations. Fixed concentrations for all species based on LLNL 2-D model or measurements	O_2, N_2, H_2O, H_2, N_2O, O_3, HNO_3 at the upper boundary (as monthly averages)	O_3, HNO_3 + NO_y; upper boundary conditions at 100 hPa
Deposition		
$\frac{\partial r}{\partial t} = K\partial^2 r(z,t)$	$V_d = \frac{1}{R_a + R_s}$	$\frac{1}{V_d} = \frac{1}{R_a} + \frac{1}{R_s} + \frac{1}{R_c}$
$\frac{K\partial r}{\partial z}(z, t) = - v_d\ r(z, t), \quad z = z_s$	V_d deposition velocity; R_a aerodynamic resistance; R_s surface resistance.	V_d deposition velocity (m s^{-1}); R_a aerodynamic resistance of the surface layer, integration of K_{zz} [*Zimmerman*, 1988] with height. R_s resistance of the laminar sub-layer between the surface and the turbulent boundary layer neglected here. R_c canopy resistance, reciprocal of stomatal conductance
r mixing ratio; K diffusion coefficient, constant 10 m^2 s^{-1}; z_s surface elevation; v_d as specific deposition velocity may vary over land and ocean; z model height	For diurnal variation: $v_{eff} = \frac{v_d}{1 + v_{dz}/k_{zz}}$	
	v_{eff} effective deposition velocity; k_{zz} vertical eddy diffusion coefficient at the first model level; z height of lowest level	
O_3, NO, NO_2, H_2O_2, HNO_3, NO_3, N_2O_5, CH_2O, CH_3OOH	O_3, NO_x, CO, CH_2O, organic peroxides	
$R_j(K) = S_j p_j(K)$	$W(K) = W_i\ 6 \times 10^{-4}\ P$	$P = \frac{\varepsilon \times R}{L}$
W_j rate of wet deposition by precipitation type j; K level; p rate of precipitation, cm/h; S_j species specific rate coefficient to account for type of precipitation; R_j ranges from 10^{-5} s^{-1} to 10^{-3} s^{-1} for precipitation rates ranging from 0.015 cm h^{-1} to 1.5 cm h^{-1}	$W(K)$ rate of wet deposition at level K; p precipitation (mm $month^{-1}$); W_i dimensionless factor; H_2O_2 1 HNO_3 2 HNO_4 0.5 CH_2O 0.7 CH_3OOH 0.5 other organic peroxides 0.7	P (s^{-1}) is corrected for less soluble species; ε dimensionless parameter describing the uptake efficiency of highly soluble species, value = 1; L(g m^{-3}) liquid water content of the rain cloud, 1 g m^{-3}; R (g m^{-3} s^{-1}) is a function of R_0, the precipitation rate at the surface; R calculated from R_0 using the function g (m^{-1}) describing the fraction of precipitation released at a given height interval calculated from the zonal mean data on the release of latent heat [*Newell et al.*, 1974]. $R(\phi, \lambda, Z, t) = R_o(\phi, \lambda, Z, t) \times g(\lambda, Z, t)$ ϕ latitude; λ longitude; Z height; t time
HNO_3, H_2O_2, N_2O_5, CH_2O, CH_3OOH, HONO	each species which was assigned a w_i (see above)	HNO_3, HNO_4, CH_2O, H_2O_2, CH_3O_2H, H_2SO_4, $(NH_4)_2SO_4$, SO_2, NH_3

[i]Other hydrocarbons.
[j]Peroxymethacrylic nitrate.
[k]*Crutzen and Gidel* [1983].
[7]*Hertel et al.* [1993].
[l]NMHC, nonmethane hydrocarbon.

Table 2. Dry Deposition Velocities V_d for the Five Models

	ECHAM[a]	GCTM[b]	GRANTOUR[c]	IMAGES[d]	MOGUNTIA[e]
			NO_2		
Land	0.25	0.25[f]	0.5	0.6 x V_d for O_3	0.25
Sea	0.1		0.1	0.1	0.1
Ice	0.1	0	0.1	0.1	—
			NO		
Land	0.04	0.25[f]	0.1	0.6 x V_d for O_3	0.04
Sea	0.0		0.1	0.1	0.0
Ice	0.0	0	0.1	0.1	—
			HNO_3		
Land	2.0	1.5[f]	1.0	2	2.0
Sea	0.8	0.3	1.0	1	0.8
Ice	0.8	0.5	0.5	0.5	—
			N_2O_5[g]		
Land	2.0	n/a	0.4	n/a	2.0
Sea	0.8		0.4	n/a	0.8
Ice	0.8	n/a	0.4	n/a	—
			NO_3		
Land	2.0	—	0.4		2.0
Sea	0.8	—	0.4		0.8
Ice	0.8	—			—
			O_3		
Land	0.4	—[h]	0.6	0.4–1[i]	0.35
Sea	0.1		0.6	0.75	0.1
Ice	0.02		0.6	0.75	
			PAN		
Land	n/a	0.25	n/a	$V_d(O_3)/3$[j]	n/a
Sea	n/a		n/a	$V_d(O_3)/3$[j]	n/a
Ice	n/a	0	n/a	$V_d(O_3)/3$[i]	n/a

Unit of measure is cm s^{-1}.

[a-e] See Table 1 footnotes a-e.

[f] These values are used when $T > 10°C$, but when $T < -10°C$, the values are the same as for ice and snow. Between -10 and +10°C V_d is linearly interpolated between the assigned values.

[g] All models which include N_2O_5 have aerosol removal (the dominant process) but not necessarily dry deposition removal.

[h] O_3 deposition is specific to land surface type [*Matthews*, 1981] and is described more fully by *Kasibhatla et al.* [1997].

[i] Deposition velocities are 0.4 cm s^{-1} on bare soils and grasslands, 0.5 cm s^{-1} on the savannah, 1 cm s^{-1} in tropical forests, and 0.6 cm s^{-1} for all other forests.

[j] IMAGES includes V_d for organic nitrates: on land $V_d = (O_3)/3$, on oceans 0.5 cm s^{-1}, and on ice and snow 0.025 cm s^{-1}.

independent of human activity and so is not relevant to this perturbation study. A large proportion of both the soil and biomass burning fluxes can be attributed to human activity. Among these five models, assumed biomass burning release of NO_x-N varies by as much as 100% (ranging from 4.7–10 Tg N yr^{-1}), reflecting the high degree of uncertainty. Assumed total soil emissions of NO_x-N also varied by more than 100% with roughly the same range (4.0–10 Tg N yr^{-1}). An even higher estimate of the global flux of NO from soil is 20 Tg N yr^{-1}, based on a compilation of available measurements [*Davidson*, 1991]; the estimate in IPCC 1994 is 12 Tg N yr^{-1} [*Prather et al.*, 1995]. Fertilizer application also substantially increases NO_x-N fluxes from soils because as much as 10–20% of fertilizer N applied to tropical agricultural soils can be returned to the atmosphere as NO_x-N [*Shepherd et al.*, 1991; *Matson et al.*, 1996; E. Veldkamp, personal comunication, 1996]. Thus, fertilizer N could contribute substantially to the total global soil NO emissions, but only the IPCC and GCTM estimates explicitly incorporate this additional source [*Shepherd et al.*, 1991; *Yienger and Levy*, 1995]. In GCTM, a much smaller percentage (2.5%) of applied fertilizer is returned to the atmosphere as NO_x. The GCTM formulation is based on analysis of measurements made in mostly temperate

Table 3. NO_x-N Sources for Five Three-Dimensional Chemical Transport Models

NO_x Emissions	ECHAM[a]	GCTM[b]	GRANTOUR[c]	IMAGES[d]	MOGUNTIA[e]
Fossil fuel	20.0	21.0	22.4	21.9	20.0
Lightning	4.0	3.0	10	8.0	5.0
Soils	10.0	5.5	5	6.7	4.0
Aircraft	—	0.45	0.23	0.44	0.6
Biomass burning	6.0	8.5	10	4.4	6.0
Stratosphere	—	0.64	0.2	0.2	—
Total	40.0	38.6	48.8	42.6	35.0

Values are in units of Tg N yr^{-1}.

[a] *Roelofs and Lelieveld* [1995].

[2] *Kasibhatla et al.* [1991, 1993], *Levy et al.* [1991], *Yienger and Levy* [1995], *Benkovitz et al.* [1996], *Levy et al.* [1996b, submitted paper, 1996].

[c] *Penner et al.* [1991, 1994].

[d] *Müller* [1992], *Müller and Brasseur* [1995].

[e] *Dentener and Crutzen* [1993].

ecosystems, and thus may be an underestimate of the fertilizer-induced NO flux [*Yienger and Levy*, 1995]. IMAGES incorporates the influence of fertilizers indirectly by tripling the emissions associated with crops in developed countries [*Müller*, 1992]. It is possible that the total global soil flux may underestimated in these models and that a substantial proportion of the global soil flux may be driven by human perturbation.

Vegetation scavenging of NO_x-N further contributes to the uncertainty amongst the estimates of soil NO_x-N fluxes. Vegetation can scavenge as much as 60–75% of the NO_x-N emitted at the soil, but this effect is represented in some of the models (MOGUNTIA and GCTM) and not in others (ECHAM or GRANTOUR) [*Bakwin et al.*, 1990a, b; *Jacob and Bakwin*, 1991; *Yienger and Levy*, 1995]. A simplistic vegetation scavenging of NO_x-N is included in the dry deposition scheme for IMAGES. Much of the overall variation in sources amongst the models results from variations in representation of the non-fossil fuel sources of NO_x-N (lightning, biomass burning, and soil emissions), many of which are influenced by human activity and so will be reflected in each model's estimate of the carbon sink.

Because of the sensitivity of the carbon sink calculation to the quantity of N deposited as well as its spatial distribution [*Townsend et al.*, 1996], we first considered fossil fuel and aircraft NO_x-N resulting in deposited NO_y-N , because their release clearly perturbs the earth's N cycle. Some proportion of the soil and biomass burning sources of NO_x-N and the animal, soil, fertilizer, and biomass burning sources of NH_x-N are also a perturbation, to incorporate these, we considered a range of proportions of non-fossil fuel-derived NO_y-N and NH_x-N as N perturbations for the carbon sink calculation. To derive a fossil fuel base case for all of the models we used the proportion of nitrogen deposition derived from fossil fuel combustion predicted by IMAGES, which tracks each of the NO_x-N sources separately, and applied that spatially distributed proportion to the total NO_y-N fields predicted by each of the five models [*Lamarque et al.*, 1996]. To estimate the proportion of total deposition which resulted from human activity, we considered the fossil fuel contribution plus 50 and 90% of total nonfossil fuel sources in our calculation of the carbon sink (the nonfossil fuel sources included are listed in Table 3). Consideration of the nonfossil fuel sources of NO_x-N contributed an additional 10 and 18 Tg of NO_y-N deposition annually for the 50% and 90% scenarios, respectively. As discussed above, estimates of important non-fossil fuel emissions of NO_x-N, which contribute substantially to NO_y-N deposition are changing considerably. We understand that an additional 18 Tg of NO_y-N deposition may be an overestimate but it reflects possible upward revisions of the global NO_x-N inventories. For NH_x-N, where the proportion of deposition that should be considered a perturbation is even less clear than it is for NO_y-N, we included 50; 60, 70, and 80% of the total NH_x-N deposition to bracket the ratio of preindustrial to industrial NH_x-N emissions of 68% calculated by *Dentener and Crutzen* [1994]. The calculated carbon storage increased linearly as the proportion of NH_x-N or NO_y-N deposition increased except when N saturation was addressed.

Time Series of NO_x-N and NH_x-N Emissions

We examined the influence of increasing nitrogen deposition over the last century by deriving a time series for both NO_x-N and NH_x-N emissions. For both cases, we scaled the emissions to a time series of global fossil fuel emissions for the last 130 years [*Keeling*, 1994; *Marland et al.*, 1994]. For 1860 to 1950, CO_2 emissions from each of the four fuel categories, coal, lignite, crude petroleum, and natural gas, were converted to NO_x-N emissions by applying the conversion factors given by *Müller* [1992]. The four categories were then summed for each year to provide the total annual estimate. For 1950–1990, the NO_x-N emissions were derived using the Müller emission factors and the country-by-country fossil fuel statistics for that reporting period. We then calculated a 0–1 scalar for each year to convert to the "current" emissions provided by each model. The resulting time series was an exponential increase in emissions over the last 130 years. We attempted to scale NH_x-N deposition to livestock populations, but, because the increase in NH_x-N emissions were driven in varying proportions by the livestock contributions, we used the same exponential increase in deposition that we used for NO_y-N.

Results and Discussion

Wet Deposition Validation

As a first step to determine whether the spatial patterns and quantities in the observations and simulations were comparable, IMAGES simulations of nitrate concentrations in precipitation were compared to the average nitrate concentration in precipitation measured at 200 sites between 1978 and 1994 as part of the U.S. National Atmospheric Deposition Program [*National Atmospheric Deposition Program*, 1995] (Figure 1). Neither the spatial distribution nor the actual quantities of nitrate deposited were adequately captured by IMAGES. First, IMAGES simulated peak deposition over the southeastern United States rather than the northeastern region (data not shown) suggesting problems with transport and rainout. Second, in a site-to-grid cell comparison, IMAGES consistently under predicted the amount of nitrate

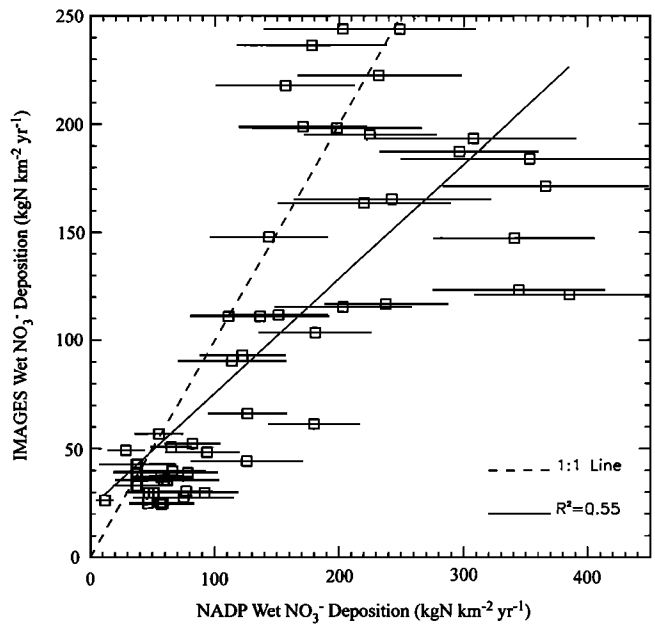

Figure 1. Comparison of NO_3^- deposition in precipitation simulated by IMAGES and NO_3^- deposition in precipitation measured at 200 sites within the United States by the NADP network [*National Atmospheric Deposition Program*, 1995]. All measurements within a 5° by 5° grid cell were averaged over the available time period (1978–1994 in most cases). Thus the bars represent the standard deviation including both the spatial and temporal variance. Note the different scales of the *X* and *Y* axes.

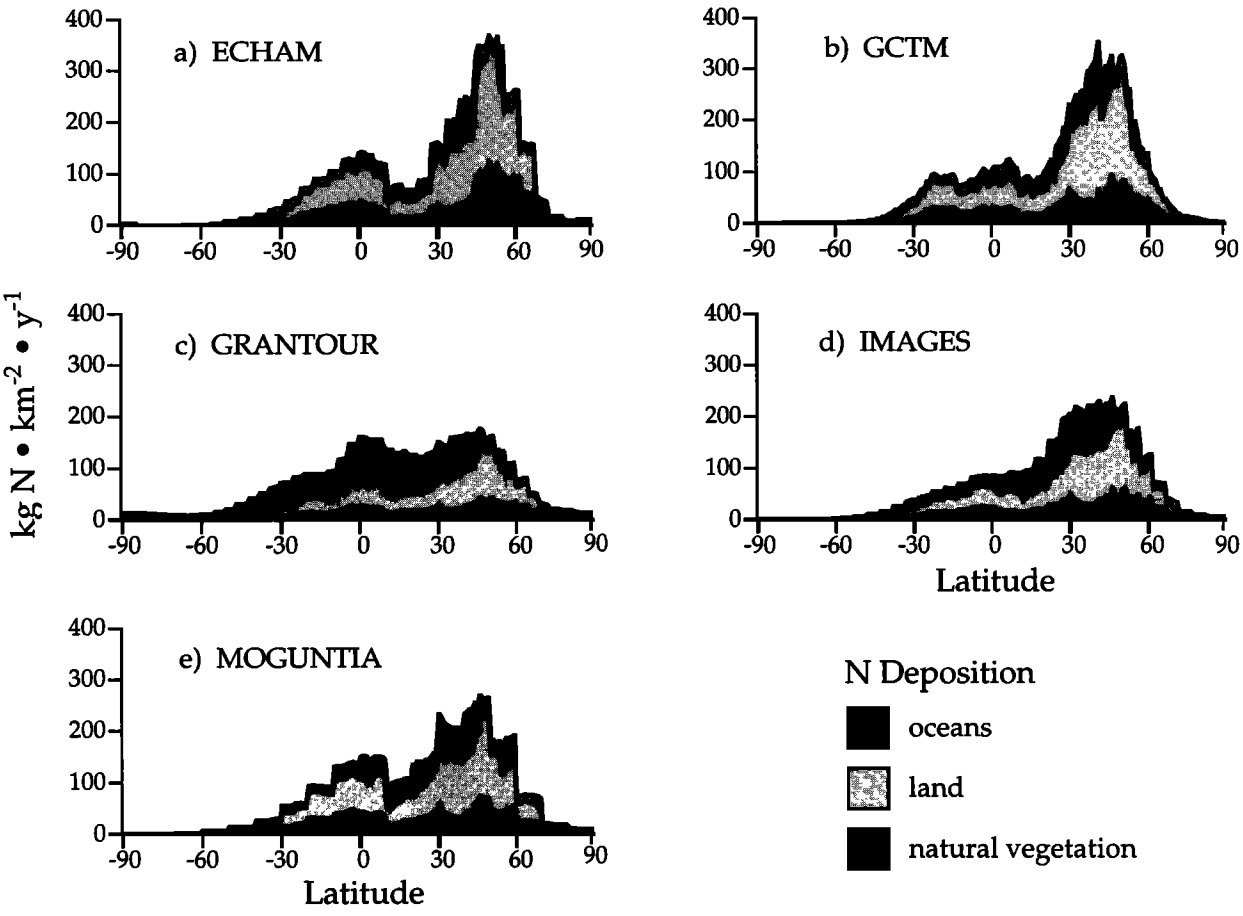

Figure 2. The latitudinal distribution of total NO_y-N deposition on oceans, land, and natural vegetation for each of the five models used. Figure 2a includes fossil fuel sources of NO_x-N only. Fossil fuel sources of NO_x-N varied by ~10% amongst the models. Figure 2b includes all sources of NO_x-N. Nonfossil fuel sources of NO_x-N vary by 100–300% (refer to Table 3 for a listing of sources).

deposited which best demonstrated by the different X and Y axes shown in Figure 1 and the r^2 of 0.55 for the relationship. A systematic bias could have been introduced into the comparison by aggregating the observations which were skewed toward lower concentrations up to the large grid cells of the simulations. It is likely that the hot spots of deposition which cover a limited area cannot be well-represented by such a large scale model. Problems with the observations [*National Atmospheric Deposition Program*, 1995] are unlikely to substantially improve the model-data comparison.

The model-data comparison suggests that transport and rainout portions of the model could be improved and such improvements are under way (J.-F. Müller, personal communication, 1996). The result is not a new one, and follows many calls for better parameterization of rainout, particularly of HNO_3, and its coupling to transport. These improvements are needed to ensure realistic simulations of atmospheric concentrations of NO_x as well as NO_y deposition [*Levy and Moxim*, 1989; *Kanakidou*, 1995; *Roelofs and Lelieveld*, 1995; *Brasseur et al.*, 1996].

The comparison was a first step toward a more systematic evaluation and illustrates the problems associated with validation of chemical transport models. Note that rainout of HNO_3 in at least one of the five models (GCTM) was parameterized using NADP data. The observation/model comparison suggests that global NO_y deposition in precipitation may be higher than simulated. Wet deposition constitutes only 40 to 60% of total N deposition, thereby weakening the model-data relationship even more [*Asman and Van Jaarsveld*, 1992; *Dentener and Crutzen*, 1994]. The following results should be interpreted knowing that, in at least one case, the details of N deposition at the spatial scale of ecosystems are simulated poorly.

Spatial Patterns of NO_y Deposition

All of the models simulated different spatial distributions and quantities of NO_y-N deposition when all sources of NO_x were considered (Figure 2b, Plate 1, and Plate 2). Differences among the models were significantly reduced when only the fossil fuel sources of NO_y-N were considered (Figure 2a and Table 4). Global N deposition generated by fossil fuel combustion varied by 10%, equal to and parallel with the variation among the assumed fossil fuel sources. The amount of NO_y-N deposition derived from fossil fuel combustion differs slightly from the sources because the proportional contributions of each source were calculated using IMAGES and applied to the individual grid cells of all of the other models. This technique provided a consistent mechanism with which to deduce the fossil fuel contribution from all of the models. Fossil fuel-derived NO_y-N is deposited mainly in the northern hemisphere, where it was released, with small amounts transported to the southern hemisphere (data not shown [*Galloway et al.*, 1994; *Lamarque et al.*, 1996]).

When all of the sources of NO_x-N were considered, the

Table 4. NO_y-N Deposition on the Earth's Surface Resulting from Fossil Fuel Combustion (Tg N yr^{-1}) Simulated by Five Three-Dimensional Transport Models and the Resulting Sink (Gt C yr^{-1}) Calculated by NDEP

	ECHAM[a]	GCTM[b]	GRANTOUR[c]	IMAGES[d]	MOGUNTIA[e]
Deposited NO_y-N from fossil fuel combustion	19.4	21.8	21.6	20.1	22.8
Oceans[f]	8.8	9.9	9.8	9.1	10.3
Land[f]	10.6	11.9	11.8	11.0	12.4
Ice or deserts[g]	0.8	0.9	0.9	0.9	1.0
Agricultural areas[g]	5.5	6.2	6.1	5.7	6.5
Natural vegetation[g]	4.3	4.8	4.7	4.4	5.0
Forests[h]	1.0	1.1	1.1	1.0	1.2
Unforested land[h]	3.3	3.7	3.6	3.4	3.8
1990 C sink[i]	0.52	0.59	0.58	0.54	0.61
1990 C sink with N saturation[j]	0.37	0.40	0.39	0.38	0.40

[a–e] See Table 1 footnotes a-e.
[f] $\sum$ (rows 2, 3) = row 1.
[g] $\sum$ (rows 4, 5, 6) = row 3.
[h] $\sum$ (rows 7, 8) = row 6.
[i] N loss = $0.2N_{av}$ (see (9)), no N saturation.
[j] N loss = $aN_{dep} + b$, where $a = 0.8/1000$ and $b = 0.2$, with N saturation.

variation in deposition increased considerably: N deposition ranged between 35.3 (IMAGES) and 41.2 (GRANTOUR) Tg N with the other models falling within this range (Figure 2, Table 5). In all cases, NO_y-N deposition was greatest between 20° and 60°N latitude; a secondary peak of varying height occurred between 10°N and 30°S latitude (Figure 2). IMAGES and GRANTOUR both deposited less N on land in the southern hemisphere than the other three models. A strong interhemispheric gradient in NO_y-N deposition was simulated by all of the models, with ECHAM and GCTM simulating the greatest northern hemisphere deposition. All of the models simulated the greatest N deposition in the eastern United States, Europe, and Asia, particularly where China faces Japan. Differences among the models are greatest in these three regions, followed by portions of Africa and South America. Interestingly, some of the difference in deposition was driven by uncertainties in the biological sources. For all models, the sum of the sources did not equal total global deposition (higher in some cases and lower in others) suggesting that N mass was not completely conserved.

Model simulations of NO_y-N deposition were similar over much of the earth's surface but localized variations in N and its partitioning over the various surface categories determined the size of the carbon sink (oceans versus land; natural vegetation versus agriculture versus ice or desert; and particularly forested versus nonforested areas, Tables 4 and 5; Plates 1and 2). With the exception of GRANTOUR, the models simulated greater N deposition on land than on oceans. Only N deposition on natural vegetation or uncultivated lands can stimulate terrestrial carbon storage because cultivated lands cannot store additional carbon per unit N deposited for the reasons described above. Furthermore, N falling on ice and deserts does not stimulate carbon uptake because there is no plant growth on ice fields, and plant growth in deserts is so limited by water availability that it is unlikely that the plants can utilize additional nitrogen to fix more carbon [*Schlesinger*, 1991]. For all five models, about 22% of NO_y-N deposition from fossil fuel combustion fell on natural vegetation, and only 5% of fossil fuel-generated NO_y-N deposition fell on forests (Table 4). The amount of fossil fuel-derived NO_y-N deposited on natural vegetation varied by 17%, slightly more than the variation in fossil fuel sources. Once expanded to include all sources of NO_x-N, the variability in spatial distribution of the deposition increased. Absolute quantities of N deposition on forests ranged from 2.2 to 4.0 Tg N yr^{-1} (Table 5). The proportion of total global N deposition received by forests, which store large amounts of carbon in wood, varied between 5.3% (GRANTOUR) and 10% (ECHAM) with IMAGES (6.6%), MOGUNTIA (8.9%), and GCTM (9%) in between. The ratio of forested to nonforested deposition varied between 0.37 (IMAGES) and 0.42 (GCTM and MOGUNTIA), with GRANTOUR (0.41) and ECHAM (0.40) falling in between. This variation in the spatial distribution of N deposition was a primary factor in determining the size and range of the resulting carbon sink when sources other than fossil fuel were considered (Plate 3 and Figure 3).

Carbon Storage from NO_y Deposition

Considering only fossil-fuel-derived NO_y-N deposition, the globally integrated annual carbon sink for all of the models ranged

Table 5. Total NO_y-N Deposition on the Earth's Surface Considering all NO_x-N Sources (Tg N yr^{-1}) Simulated by Five Three-Dimensional Chemical Transport Models

	ECHAM[a]	GCTM[b]	GRANTOUR[c]	IMAGES[d]	MOGUNTIA[e]
Global NO_y-N deposition	38.9	40.2	41.2	35.3	39.9
Oceans[f]	11.7	12.6	25.8	16.2	14.9
Land[f]	27.2	27.6	15.4	19.1	25.0
Ice or deserts[g]	1.2	1.2	1.2	1.4	1.4
Agricultural areas[g]	12.2	14.1	6.6	8.9	11.4
Natural vegetation[g]	13.8	12.3	7.7	8.8	12.1
Forests[h]	4.0	3.6	2.2	2.3	3.6
Unforested land[h]	9.8	8.6	5.4	6.5	8.5

[a–e] See Table 1 footnotes a-e.
[f–h] See Table 4 footnotes f-h.

from 0.52 to 0.61 Gt C yr^{-1} (Table 4) for 1990. For the decade of the 1980s, the average global terrestrial C sink ranged from 0.48 to 0.56 Gt C yr^{-1} with a 15–20% difference between the minimum and the maximum values. These values represent approximately 25–33% of the "missing sink" [*Schimel et al.*, 1995; *Schimel*, 1995]. When additional sources of NO_x-N were considered, the variation in the size of the estimated carbon sink grew to 100%, and partially depended on the proportion of nonfossil fuel sources of NO_x-N considered (Table 5; Figure 3a). When fossil fuel sources of NO_x-N plus 50% of nonfossil sources of NO_x-N were considered, the 1990 calculated carbon sink ranged from 0.65 Gt C yr^{-1} for GRANTOUR to 0.97 Gt Cyr^{-1} for ECHAM (Figure 3a), and the average global terrestrial carbon sink for the 1980s ranged from 0.61 to 0.87 Gt C yr^{-1}. When fossil fuel sources of NO_x-N plus 90% of nonfossil sources of NO_x-N were considered, the 1990 calculated carbon sink ranged from 0.72 Gt C yr^{-1} for GRANTOUR to 1.34 Gt C yr^{-1} for ECHAM (Figure 3a), and the average global terrestrial carbon sink from the 1980s ranged from 0.66 to 1.23 Gt C yr^{-1}. The size of the carbon sink was proportional to the amount of N deposited on natural vegetation and was closely linked to the amount of N deposited on forests because carbon storage in wood dominates all other storage compartments (Tables 4 and 5 *Townsend et al.* [1996]). The relatively small proportion of total global N deposition that fell on forests (<10%) was the most important factor determining the size of the carbon sink (Table 5 [*Townsend et al.*, 1996]).

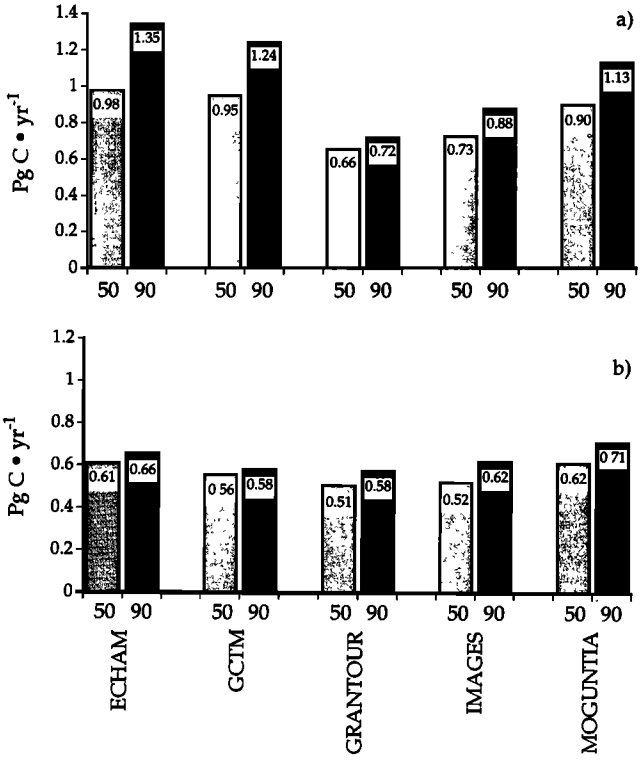

Figure 3. Globally integrated carbon storage calculated by NDEP from NO_y-N deposition considering NO_x-N emissions from fossil fuel combustion plus 50% and 90% of nonfossil fuel sources for each of the five models. (a) Plot of *n*loss= 0.2 N_{av} and 80% of the nitrogen deposited is assimilated by the ecosystem receiving it and used to fix carbon. The remaining 20% is assumed to be transferred back to the atmosphere as NO, N_2O, or N_2 or to hydrologic systems. (b) Plot of *n*loss= a + bN_{av}, where a is 0.8/1000 and b is 0.2. Modeled ecosystems utilized an increasingly smaller proportion of the nitrogen deposited up to a maximum, considered the N saturation case. See text for further discussion.

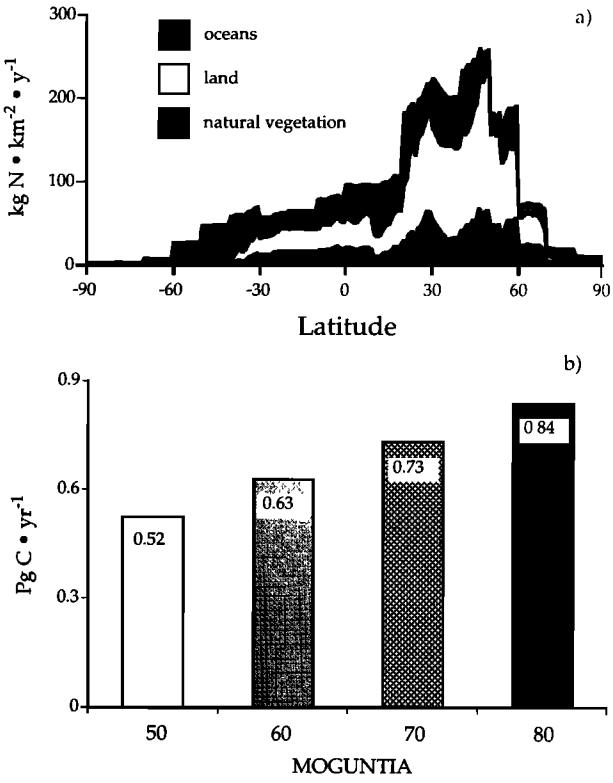

Figure 4. (a) Latitudinal distribution of total NH_x-N deposition on the Earth's surface including oceans, land, and natural vegetation. (b) Globally integrated carbon storage calculated by NDEP considering 50%, 60%, 70%, and 80% of the NH_x-N deposition simulated by MOGUNTIA [*Dentener and Crutzen*, 1994]. The carbon sink calculations assumed no N saturation and 80% of the available N was assimilated into biomass carbon and nitrogen as in Figure 3a.

Effects of NH_x Deposition

Emissions of ammonia and ammonium (NH_x-N) represent at least as large a flux of N to the atmosphere as NO_x-N [*Dentener and Crutzen*, 1994]. As pointed out in Table 2, global NO_x-N emissions to the atmosphere are estimated to be 35 to 49 Tg N yr^{-1} for the five models and NH_x-N emissions are estimated to be 45 Tg N yr^{-1} [*Dentener and Crutzen*, 1994]. The only three-dimensional chemical model to date that considers ammonia is a updated version of MOGUNTIA developed by *Dentener and Crutzen* [1994]; we used this version to estimate the size of the carbon sink from NH_x-N. Total NH_x-N deposition in this model version was 41 Tg N yr^{-1} due to a somewhat smaller ocean source. As with NO_y-N deposition, NH_x-N deposition was greater on land (22.5 Tg N yr^{-1}) than on oceans (18 Tg N yr^{-1}) (Figure 4a). The partitioning of NH_x-N deposition between the various land categories was: 1.2 Tg N yr^{-1} on ice or deserts, 11 Tg N yr^{-1} on agriculture, and 10.1 Tg N yr^{-1} on natural vegetation, which could be further partitioned into 7.3 Tg N yr^{-1} on nonforested land and 2.9 Tg N yr^{-1} on forests. Thus, only 7.1% of the total NH_x-N deposited fell on forests. The partitioning of NH_x-N deposition

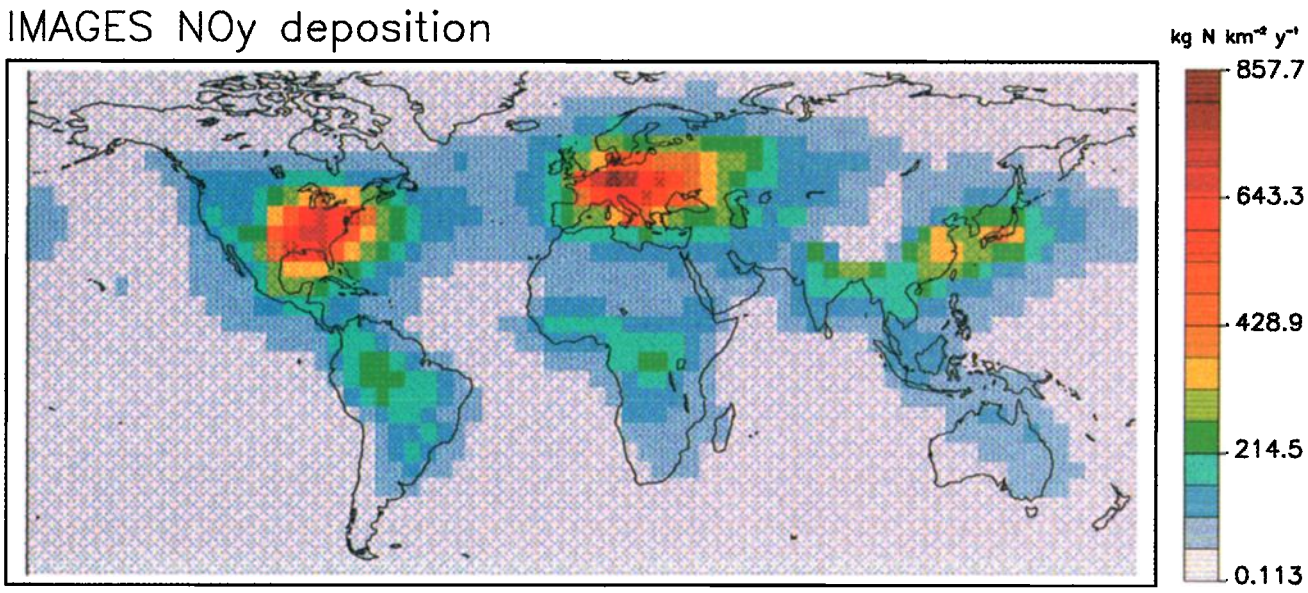

Plate 1. Global distribution of total NO_y-N deposition simulated by IMAGES in kg N km^{-2} yr^{-1}.

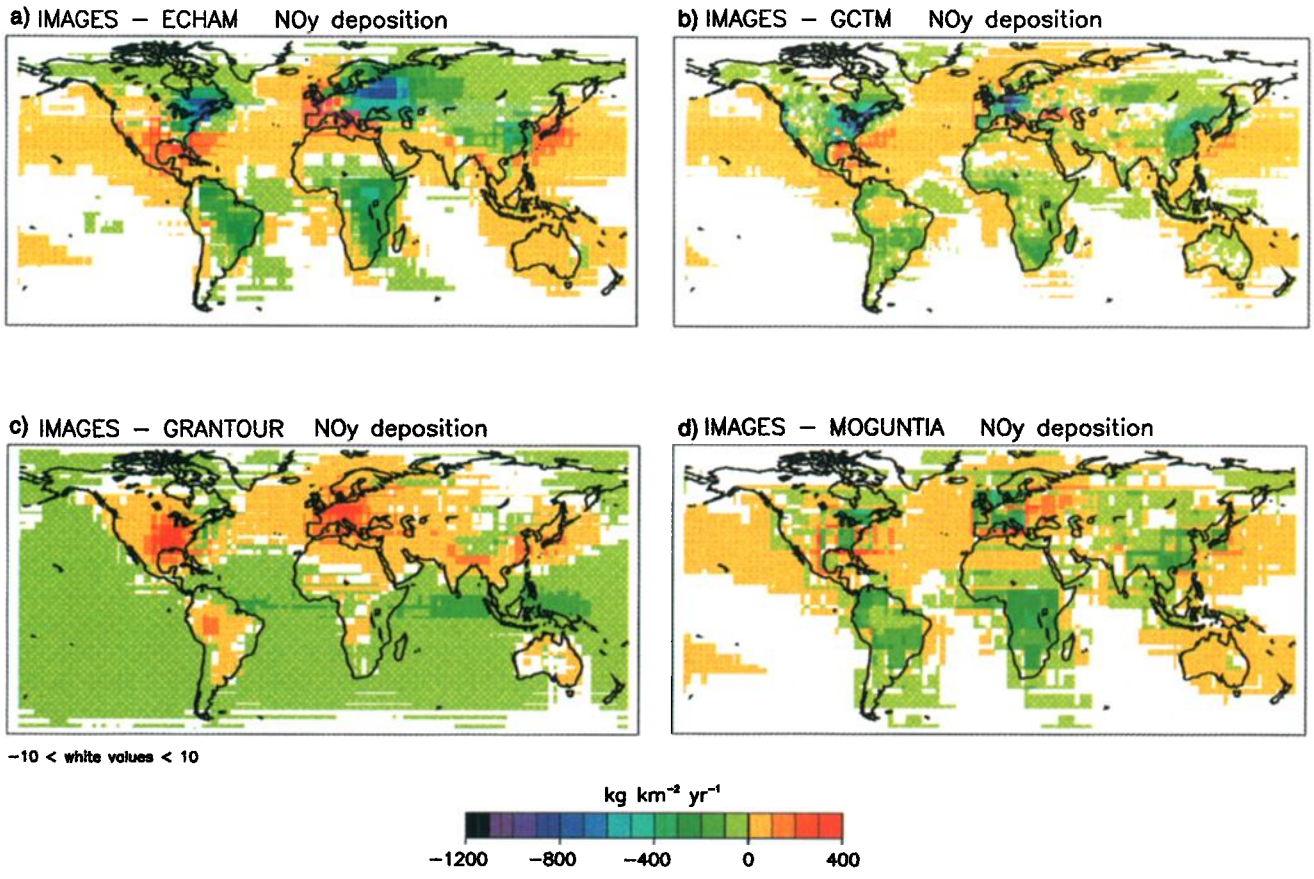

Plate 2. Global distributions of the difference between total NO_y-N deposition simulated by IMAGES and each of the other models: (a) IMAGES minus ECHAM, (b) IMAGES minus GCTM, (c) IMAGES minus GRANTOUR, and (d) IMAGES minus MOGUNTIA. All of the differences were calculated based on a 1° by 1° map of the deposition fields. Warm colors indicate areas where IMAGES N deposition was greater than the other model, and cool colors indicate areas where the other model predicted greater N deposition than IMAGES. Areas mapped as white differed from IMAGES by less than 10 kg N km^{-2} yr^{-1}.

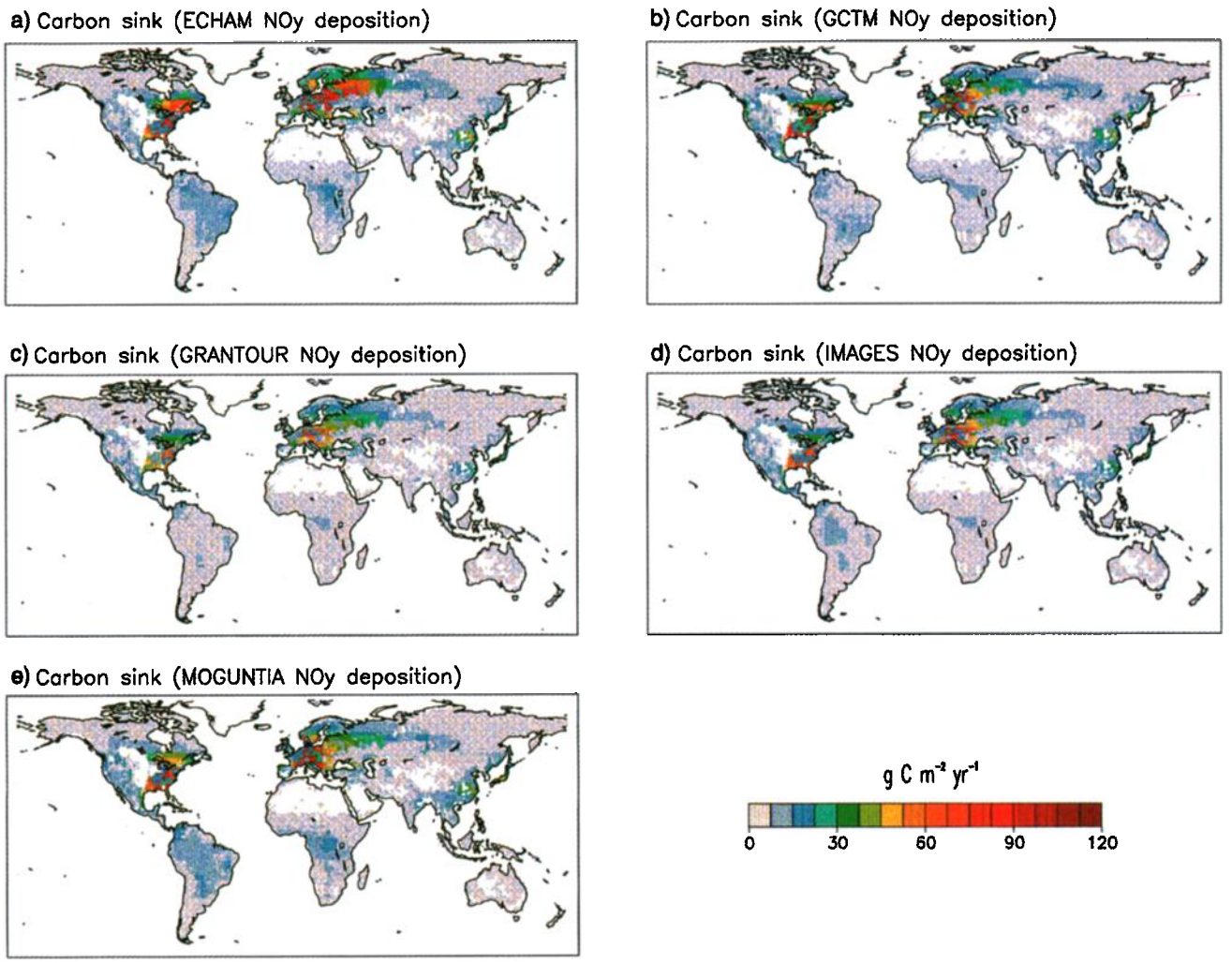

Plate 3. Global distributions of carbon storage simulated by NDEP for NO_y-N deposition from fossil fuel combustion + 50% of the nonfossil fuel NO_x-N sources: a) ECHAM, b) GCTM, c) GRANTOUR, d) IMAGES, and d) MOGUNTIA. All NDEP simulations were done on a 1° by 1° grid determined by *Matthews'* [1983] vegetation map and the deposition fields were simply regridded rather than smoothed to reduce bias among the model comparisons.

was likely to have been influenced by specific attributes of MOGUNTIA and its parameterization. First, MOGUNTIA applies a dry deposition factor of 25% to anthropogenic NH_x-N emissions to account for subgrid deposition within the rather large 10° by 10° grid cells. While this may result in overestimation of NH_x-N deposition in some nonagricultural areas, the uncertainties associated with the actual NH_x-N emission estimates are likely to override any bias in deposition introduced by the anthropogenic deposition parameterization. For example, *Schlesinger and Hartley* [1992] estimate global NH_3-N emissions to be 75 Tg N yr^{-1}, substantially greater than the 45 Tg N used here (emissions were greater in almost every category: animal, soil, fertilizer, and oceanic sources). *Galloway et al.* [1995] estimated NH_x-N emissions to be 68 Tg N annually. Second, in some areas of the world and particularly in the tropics, domestic animals eat an unknown proportion of natural vegetation; NH_x-N emitted from the processing and excretion of that natural vegetation should be not be considered a perturbation for our carbon sink calculation. Despite these concerns, MOGUNTIA has examined the consistency of estimated emissions with measured deposition to produce an internally consistent look at the global NH_x-N cycle.

The size of carbon sink induced by the deposition of NH_x-N emissions ranged from 0.52 to 0.84 Gt C yr^{-1}, depending on the proportion of the deposition included, from a low of 50% to a high of 80% (Figure 4b). NH_x-N emissions have risen exponentially over the last century [*Nevison et al.*, 1996], and clearly, some proportion of the emissions, which are largely derived from agricultural and animal husbandry activities, represent an increase over preindustrial times when the earth supported a much smaller population of humans. However, the exact emissions proportion attributable to human activity is extremely difficult to assess. *Dentener and Crutzen* [1994] estimated that anthropogenic emissions were 30.6 out of the 45 Tg N emitted per year, or 68%, and *Galloway et al.* [1995] arrived at an estimate of 69%. The spatial distribution of NH_x-N deposition and the resulting sink were different than those generated for NO_y-N deposition (Plate 4). The most striking difference was the increase in N deposition in tropics, particularly in the northern tropics: India, China, Central America, and northern South America. Consistent with this, the consideration of NH_x-N emissions resulted in increased N deposition between 30° and 45°N latitude compared to NO_y deposition. As a result, N deposition intensified for the low

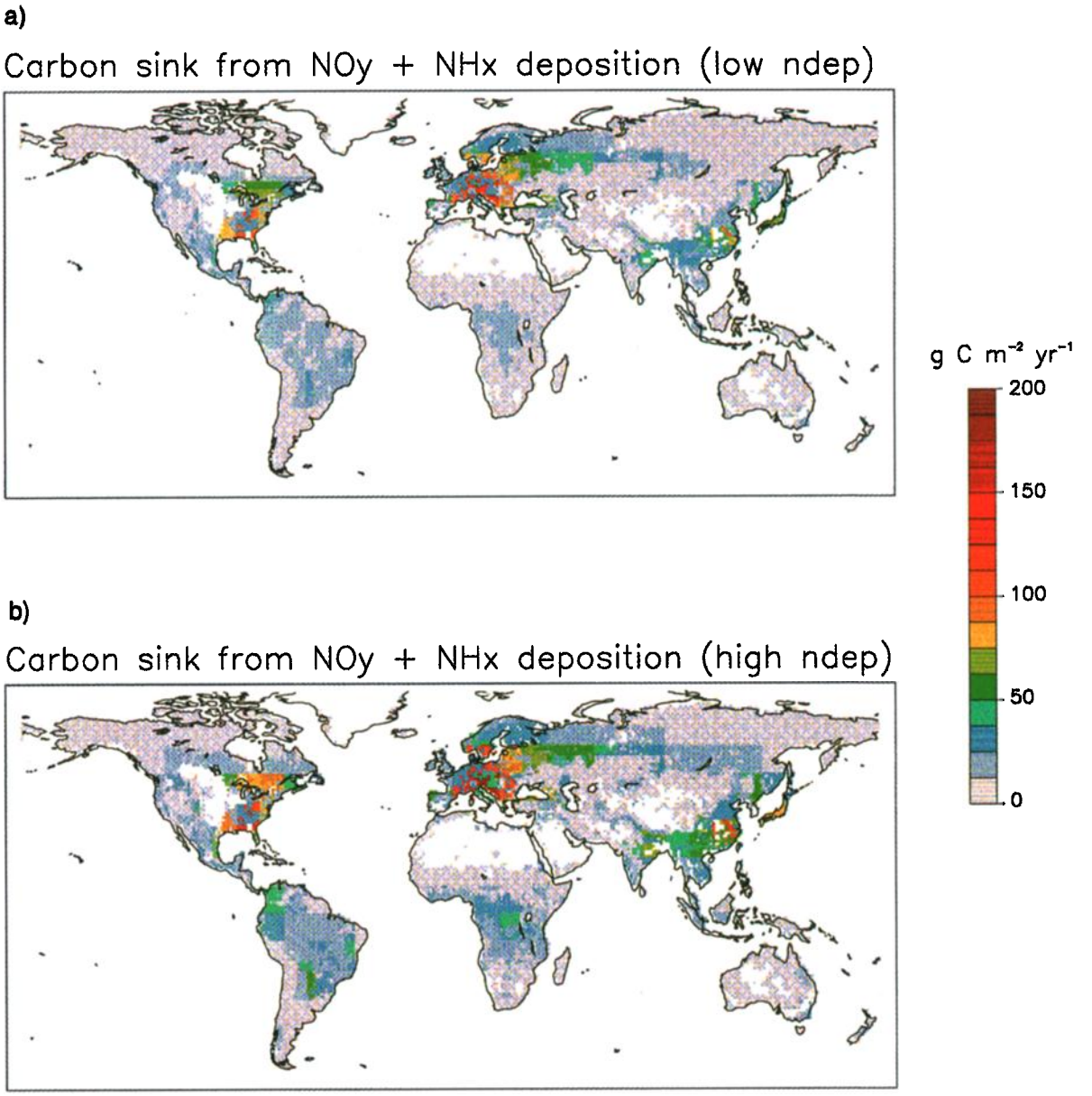

Plate 4. Map of the global distribution of carbon storage calculated by NDEP considering both the NO_y-N and NH_x-N simulated by MOGUNTIA. Plate 4a considers fossil fuel emissions + 50% of nonfossil fuel sources and 50% of the N deposited from NH_x-N emissions. Plate 4b considers fossil fuel emissions + 90% of nonfossil fuel sources and 95% of the N deposited from NH_x-N emissions. For both runs, we assumed no N saturation and that 80% of the available N was assimilated into biomass carbon and nitrogen ($n$loss = 0.2 N_{av}, as in Figure 3a). Globally integrated carbon storage ranged from 1.19 to 1.6 Gt C annually for the two cases.

latitudes of the northern hemisphere for NH_x-N relative to NO_y deposition which mimics the animal distributions. North of 40°N the pattern of NH_x-N deposition was very similar to that of NO_y-N deposition due to a mix of agriculture and industry in the northern temperate zone (Figure 4a) [*Chameides et al.*, 1994]. Estimates of the annual global flux of NH_x-N are uncertain and the larger estimates could generate a still larger carbon sink depending on its spatial distribution. As with NO_y-N deposition, NH_x-N has the potential to generate a substantial stimulation of terrestrial carbon uptake. We estimate that this uptake is likely to be larger than 0.50 Gt C yr^{-1}. When both NO_y-N and NH_x-N were included, our C uptake estimates grew to 1.42 to 1.97 Gt Cyr^{-1} and the decadal average for 1980s grew to between 1.31 and 1.81 Gt C yr^{-1}. The NO_y-N perturbation included fossil fuel sources of NO_x-N and 50 and 90% of the nonfossil fuel sources respectively, and the NH_x-N perturbation included 50 and 80% of the total NH_x-N sources, respectively. In addition, we assumed that C fixation was not hampered due to N saturation in regions of high chronic deposition. The inclusion of N saturation, reflecting negative feedbacks such as high O_3 and acidification, severely constrained modeled CO_2 uptake (reducing C uptake by between 0.34 and 0.62 Gt C yr^{-1}) and might eventually constrain C uptake for the ever expanding polluted regions of the world [*Chameides et al.*, 1994; *Townsend et al.*, 1996].

Constraints on Ecosystem Productivity

It is well known that nitrogen deposition is not only a fertilizing agent for terrestrial vegetation, but depending on the source, will be associated with acid precipitation and high ozone concentrations, both of which alter ecosystem function [*Reich*, 1987; *Aber et al.*, 1989; *McLaughlin and Downing*, 1995]. Because these chemical changes to the environment result in reduced photosynthesis and/or plant growth, they also act to reduce the incorporation of additional N into biomass and soil organic matter. Chronic nitrogen deposition may simply result in limitation by some other nutrient or abiotic factor. These ecosystem-level constraints that halt fertilization by pollutant N are collectively known as nitrogen saturation, and are associated with high N losses from nitrification, denitrification, and leaching, as well as reduction of fine roots and mycorrhizae. Under extreme loading, such as that observed in central and eastern Europe and parts of the northeastern United States, ecosystems may become saturated. Recent studies of Norway spruce forests in northeastern Bavaria showed that six stands receiving an average of 2,105 kg N km^{-2} yr^{-1} in atmospheric N deposition were suffering slight to serious forest decline while two nearby stands receiving an average of 2,051 kg N km^{-2} yr^{-1} in atmospheric N deposition remained healthy [*Durka et al.*, 1994]. A modeling study of alpine ecosystems in the Colorado Rockies suggested that the ecosystems would begin to lose their ability to retain N and that the N would end up in stream water when N deposition exceeded 1600 kg N km^{-2} yr^{-1} [*Baron et al.*, 1994].

To consider how N saturation might influence terrestrial carbon uptake, we followed the same procedure outlined in *Townsend et al.* [1996]. Up to this point of the study, our calculations assumed continuing N-limitation by all terrestrial ecosystems, so that an increment in available N due to deposition results in an increment in carbon storage (Figure 3a) [*Townsend et al.*, 1996]. Net storage for a model of deposited N is thus only a function of the C:N ratios and multiple turnover times of the ecosystem components. To begin to address the possible implications of nitrogen saturation on the N-induced C sink, we conducted a set of NDEP simulations that included a simple parameterization of a reduction in ecosystem nitrogen use efficiency (NUE) in response to chronic deposition. Retention of available N (including deposited and recycled N) was inversely proportional to the amount of N deposited. The fraction of N retained was decreased linearly as a function of deposition down to a critical threshold where inputs were equal to outputs and none of the additional deposited N was retained by the ecosystem. The result was to effectively place a cap on the N-induced carbon sink between 0.5 and 0.6 Gt yr^{-1} (Figure 3b).

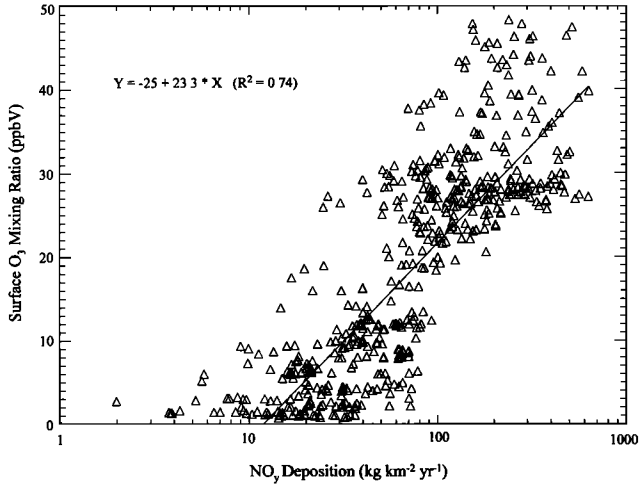

Figure 5. Annual average ozone concentration in the surface layer of IMAGES (900 mbar) compared to the predicted NO_y-N deposition (kg N km^{-2} yr^{-1}) including both wet and dry deposition of N. The comparison was limited to those grid cells containing natural vegetation.

Tropospheric ozone is probably the most harmful pollutant to terrestrial vegetation, interfering with many physiological processes including photosynthesis, respiration, and allocation [*Reich*, 1987; *Chameides et al.*, 1994] The net effect is a reduction in growth. We did not explicitly model O_3 damage, but Figure 5 shows that surface O_3 concentrations and NO_y-N deposition are correlated and so O_3 may limit carbon storage response at high levels of N deposition. In this study, both surface O_3 mixing ratios and NO_y-N deposition are annual averages over large grids and are underestimated (see above [*Müller and Brasseur*, 1995]), which results in few O_3 concentrations above the critical threshold of between 50 and 70 ppbv [*Chameides et al.*, 1994]. Both the spatial and temporal averaging may contribute to the underestimation. However, the correlation between O_3 concentration and NO_y-N deposition illustrates that chemical feedbacks that could be represented by the individual mechanisms of soil acidification, ozone damage, alleviation of N limitation, and the added influence of sulfur deposition, serve as non-linear interacting regulators of terrestrial carbon fixation. We implemented a rudimentary parameterization of these collective effects as described above, but the underlying mechanisms deserve further attention.

Relation of This Study to Other Analyses

This study is only the second study to explicitly consider the spatial distribution of nitrogen deposition on ecosystems [*Townsend et al.*, 1996]. In *Peterson and Melillo's* [1985] publication, their estimate of carbon uptake by the forest vegetation and soils due to N fertilization was 100 Tg C yr^{-1} or 0.1 Gt C yr^{-1}, a relatively small sink and less than one-fifth our current estimate for either NO_y-N or NH_x-N deposition and less than one-tenth of our total carbon sink estimate. They assumed that a total of 6 Tg out of 20 Tg N released by fossil fuel combustion was deposited on natural vegetation which was slightly higher than our estimate of 4.3–5.0 Tg NO_y-N from fossil fuel combustion (Table 4). The present study is distinguished by (1) simulation of the N metabolism of specific land cover types including forests, grasslands, tundra, and cultivated lands; (2) derivation of the spatial distribution of N deposition using chemical transport models; (3) evaluation of the cumulative effect of rising N deposition and recycling of deposited N; (4) an assumption that 80% of the deposited N is retained, compared with *Peterson and Melillo* [1985], who assumed 60% retention when N saturation was not considered; and (5) the incorporation of C:N ratios for different pools, which reflect the intervening decade of measurements and resulting understanding. No single difference can be identified as the most important, but rather it is the combination of all of the factors.

More recent estimates of the carbon sink generated by anthropogenic N deposition range from 0.50 to 1.50 Gt C yr^{-1} [*Kohlmaier et al.*, 1988; *Schindler and Bayley*, 1993; *Hudson et al.*, 1994; *Townsend et al.*, 1996]. *Hudson et al.* [1994] simulated a carbon sink of ~1.4 Gt C yr^{-1} with N deposition of 18 Tg N yr^{-1} to temperate and boreal forests. The five chemical transport

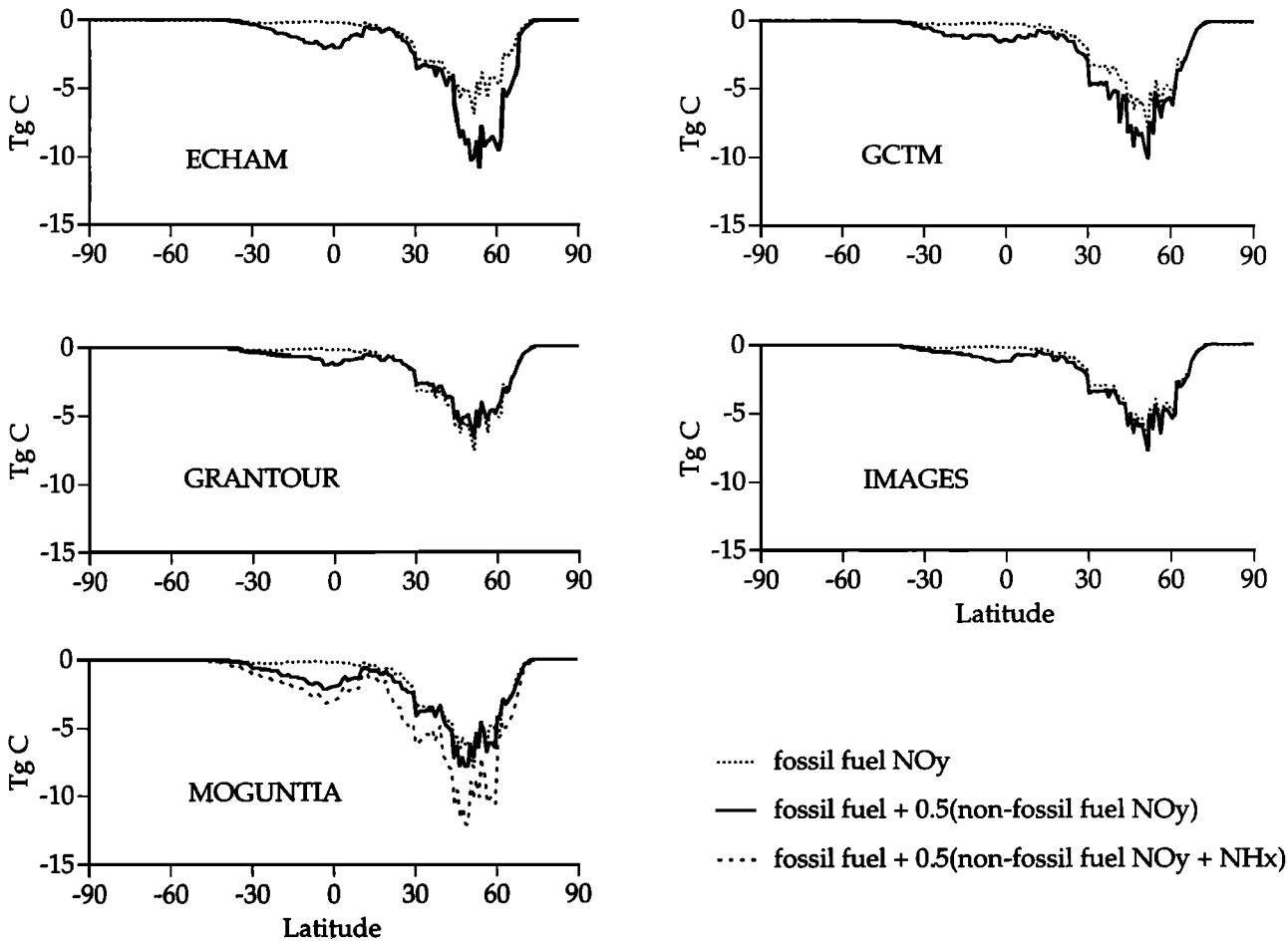

Figure 6. Latitudinal distribution of the carbon sink considering NO_y-N deposition derived from fossil fuel combustion and considering NO_y-N deposition derived from fossil fuel combustion plus 50% of the nonfossil fuel sources for each of the five models. For MOGUNTIA, we consider NO_y-N deposition derived from fossil fuel combustion plus 50% of the nonfossil fuel sources plus 50% of the NH_x-N deposition. The carbon sink calculations assumed no N saturation and that 80% of the available N was assimilated into biomass carbon and nitrogen.

models studied here simulate between 2.2 and 4 Tg N yr^{-1} as NO_y-N and 2 Tg N yr^{-1} as NH_x-N on all forests, including temperate, boreal, and tropical forests (fossil fuel plus all other sources, Table 5). *Schindler and Bayley* [1993] estimated a carbon sink of between 0.65 and 1.95 on land, depending on the assigned C:N of the terrestrial biosphere and assuming global N deposition on land of 13 Tg N yr^{-1}, which is similar to our fossil fuel NO_y-N estimate of between 10.6 and 12.4 Tg N yr^{-1} deposited on land globally. The estimates of both *Schindler and Bayley* [1993] and *Hudson et al.* [1994] differ from ours in the assignment of C:N ratios, assumptions about the geography of N deposition and ecosystems, and neglect of N recycling.

The analysis of atmospheric CO_2 and $^{13}C\,O_2$ has provided another perspective on the global carbon cycle and has allowed a more robust determination of the latitudinal distribution of the net terrestrial CO_2 exchange [*Ciais et al.*, 1995] There is general agreement in the pattern of the time series of the N deposition terrestrial carbon sink and that calculated by difference within the global carbon budget (data not shown) [*Schimel et al.*, 1995]. However, there is much less year to year variability in the N deposition induced terrestrial carbon sink because we do not include interactions with climatic variability in our model. Recent analyses suggest that year to year variability in the size of terrestrial carbon sink is determined by interactions between the climate and the nitrogen cycle [*Braswell*, 1996; *Schimel*, 1996]. The latitudinal distribution of the carbon sink derived from N deposition is similar to the latitudinal distribution derived from the isotopic measurements (Figure 6 [*Ciais et al.*, 1995]). The inverse estimates suggest a northern hemisphere midlatitude terrestrial sink, which all of our estimates also show (Table 6). When we include the nonfossil fuel NO_x and NH_x sources, southern subtropical carbon uptake is similar to that estimated by *Ciais et al.*[1995]. The intensity of both the northern hemisphere and subtropical C sinks varies among the models, with GCTM, ECHAM, and MOGUNTIA showing the strongest northern hemisphere sink and ECHAM and MOGUNTIA showing the strongest subtropical sinks. While the resemblance of the latitudinal distributions of the C sink may be coincidental, if the nitrogen deposition-induced carbon sink generated a latitudinal distribution clearly inconsistent with data-based inverse estimates, the mechanism could be neglected. The apparent agreement suggests that the role of N deposition in the carbon cycle should be investigated further, using empirical as well as more mechanistic modeling approaches.

The N-induced C sink estimate of 1.42 to 1.97 Gt C yr^{-1} reflects our current understanding of both atmospheric chemistry and

Table 6. Comparison of Terrestrial Net CO_2 Flux Estimated by Inverse Deconvolution and Our Perturbation Estimate of Terrestrial Net CO_2 Flux from N Deposition

	90°S–16°S	Equatorial	16°N–90°N	Global
Keeling et al. [1989] [a]	-0.1	+0.3	-0.6	-0.5
Tans et al. [1994] [a]	-0 1	+0.5	-2.3	-1.9
Ciais et al. [1995] [b]	-0.2	+0.8	-2.2	-1.5
	With Saturation			
This work				
IMAGES [c]	-0.04	-0.11	-0.38	-0.53
ECHAM [c]	-0.05	-0.16	-0.41	-0.62
GCTM [c]	-0.06	-0.13	-0.37	-0.56
GRANTOUR [c]	-0.04	-0.11	-0.36	-0.51
MOGUNTIA [c]	-0.05	-0.16	-0.40	-0.61
MOGUNTIA $NH_x + NO_y$ [d]	-0.10	-0.26	-0.73	-1.09
	Without Saturation			
This work				
IMAGES [c]	-0.04	-0.12	-0.57	-0.73
ECHAM [c]	-0.05	-0.19	-0.73	-0.97
GCTM [c]	-0.07	-0.15	-0.73	-0.95
GRANTOUR [c]	-0.04	-0.12	-0.50	-0.66
MOGUNTIA [c]	-0.06	-0.20	-0.64	-0.90
MOGUNTIA $NH_x + NO_y$ [d]	-0.11	-0.29	-1.02	-1.42

Values are in units of Gt C yr^{-1}.
[a]Based on CO_2 concentrations.
[b]Based on $^{13}CO_2 + CO_2$.
[c]Includes NO_y deposition from fossil fuel combustion and 50% of nonfossil fuel NO_y.
[d]Includes NO_y deposition from fossil fuel combustion and 50% of nonfossil fuel NO_y plus 50% of NH_x deposition.

ecological function but requires a comprehensive critical evaluation to determine if it is realistic and could persist through time. This range is determined entirely by the proportion of N deposition to consider as a perturbation and does not include the considerable uncertainties of ecological processes. Outstanding examples that can substantially influence the size of the carbon sink include the mapping of vegetation types, the amount of carbon assimilation allocated to woody biomass, and the issue of nitrogen saturation and potential chemical feedbacks outlined above [*Townsend et al.*, 1996]. Sensitivity analyses of these factors generate as large or larger ranges in the size of the C sink estimate. Improved carbon sink estimates will be available only through an increased understanding of both atmospheric chemistry and its influence on terrestrial ecosystem function.

Conclusions

The carbon cycle and nitrogen deposition have been treated as separate issues scientifically and politically. We have argued that they are coupled and that the effects of changing atmospheric CO_2, N, and O_3 on the biosphere are highly interactive. Terrestrial sinks are not independent of one another. Nitrogen fertilization by N deposition may have provided sufficient N to allow the stimulation of northern hemisphere forest regrowth [*Houghton and Meira Filho*, 1994; *Schimel*, 1995]. Increased N availability for plant growth resulting from N deposition may have provided the supplemental N needed to sustain growth under elevated CO_2 [*Amthor*, 1995; *Schimel*, 1995]. Climate variability can modulate all of the other mechanisms. The challenge for all analyses of the processes contributing to terrestrial carbon uptake is to develop estimates that include the overlapping, nonlinear and possible inverse feedbacks, and potential constraints on ecosystem productivity.

The size of the N sources (including both NH_x-N and NO_y-N) were proportional to N deposition on land and natural vegetation, but less than 10% of the global nitrogen deposition fell on forests, which played the most important role in carbon storage. In general, as N deposition increased in a region and over time, the greater the carbon storage. However, this is not true for areas where land use change has converted land to agriculture or otherwise produced ecosystems lacking in woody vegetation. Also, the introduction of N saturation greatly reduced the size and persistence of the carbon sink, and the sink was no longer proportional to N deposition, but the remaining carbon sink was still large enough to play a significant role in the global carbon cycle. Because O_3 concentrations and nitrogen deposition are spatially correlated, O_3 may limit terrestrial carbon uptake due to N deposition. Narrowing uncertainties in both the ecological influences of N deposition and its atmospheric chemistry and transport will translate directly into a better understanding of the changing bio-atmospheric cycles of carbon and nitrogen. Future uptake of carbon by the terrestrial biosphere will be less with either N saturation or O_3 pollution feedbacks. If N fertilization of the terrestrial biosphere is the "missing C sink" or a substantial portion of it, we would expect significant reductions in its magnitude over the next century.

Acknowledgments. The authors are grateful for funding provided by the National Science Foundation, which sponsors the National Center for Atmospheric Research, the National Aeronautic and Space Administration through the Process Studies Program (1364-CAR91-008) and the Earth Observing System (NAGW-2662), and the National Institute for Global Environmental Change (TUL-039-95/96) funded by the Department of Energy (DOE). James Galloway's provocative questions provided the catalyst for this study. B. H. Braswell was supported by a DOE Global Change Graduate Student Fellowship, and A. R. Townsend was supported by a UCAR postdoctoral fellowship in Global Change Studies funded by the National Oceanic and Atmospheric Administration (NOAA). Jason Neff, David Schimel, Susan Solomon, Elizabeth Sulzman, and two anonymous reviewers provided thorough and thoughtful reviews.

References

Aber, J. D., K. J. Nadelhoffer, P. Steudler, and J. M. Melillo, Nitrogen saturation in northern forest ecosystems, *BioScience*, *39*(6), 378-386, 1989.

Amthor, J. S., Terrestrial higher-plant response to increasing atmospheric [CO_2] in relation to the global carbon cycle, *Global Change Biol.*, *1*(4), 243-274, 1995.

Asman, W. A. H., and H. A. Van Jaarsveld, A variable-resolution transport model applied for NH_x in Europe, *Atmos. Environ.*, *26A*, 445-464, 1992.

Bakwin, P. S., S. C. Wofsy, and S. M. Fan, Measurements of reactive nitrogen oxides (NO_y) within and above a tropical forest canopy in the wet season, *J. Geophys. Res.*, *95*, 16,765-16,772, 1990a.

Bakwin, P. S., S. C. Wofsy, S. M. Fan, M. Keller, S. Trumbore, and J. M. de Costa, Emission of nitric oxide (NO) from tropical forest soils and exchange of NO between the forest canopy and atmospheric boundary layers, *J. Geophys. Res.*, *95*, 16,755-16,764, 1990b.

Baron, J. S., D. S. Ojima, E. A. Holland, and W. J. Parton, Analysis of nitrogen saturation potential in Rocky Mountain tundra and forest: Implications for aquatic systems, *Biogeochemistry*, *27*, 61-82, 1994.

Bauer, A., and A. L. Black, Effect of tillage management on soil organic carbon and nitrogen, *Farm Res.*, *40*(6), 27-31, 1983.

Benkovitz, C. M., M. T. Scholtz, J. Dignon, J. Pacyna, T. Acholtz, L. Tarrason, E. M. Voldner, and T. E. Graedel, Global gridded inventories of anthropogenic emissions of sulfur and nitrogen, *J. Geophys. Res.*, *in press*, 1996.

Brasseur, G. P., D. A. Hauglustaine, and S. Walters, Chemical compounds in the remote Pacific troposphere: Comparison between MLOPEX measurements and chemical transport model calculations, *J. Geophys. Res.*, *101*, 14,795-14,813, 1996.

Braswell, B. H., Global terrestrial biogeochemistry: Perturbations, interactions, and time scales, Ph.D. thesis, Univ. of N.H., Durham, 1996.

Chameides, W. L., P. S. Kasibhatla, J. Yienger, and H. Levy II, Growth of continental-scale metro-agro-plexes, regional ozone pollution, and world food production, *Science*, *264*, 74-77, 1994.

Ciais, P., P. P. Tans, J. W. C. White, M. Trolier, R. J. Francey, J. A. Berry, D. R. Randall, P. J. Sellers, J. G. Collatz, and D. S. Schimel, Partitioning of ocean and land uptake of CO_2 as inferred by $\delta^{13}C$ measurements from the NOAA Climate Monitoring and Diagnostics Laboratory Global Air Sampling Network, *J. Geophys. Res.*, *100*, 5051-5070, 1995.

Crutzen, P. J., and L. T. Gidel, A two-dimensional photochemical model of the atmosphere, 2, The tropospheric budgets of the anthropogenic chlorocarbon, CO, CH_4, CH_3Cl and the effect of various NO_x sources on tropospheric ozone, *J. Geophys. Res.*, *88*, 6641-6661, 1983.

Davidson, E. A., Fluxes of nitrous oxide and nitric oxide from terrestrial ecosystems, in *Microbial Production and Consumption of Greenhouse Gases: Methane, Nitrous Oxides, and Halomethanes*, edited by Rogers, J.E., and Whitman, W.E., pp. 219-236, Am. Soc. for Microbiol., Washington, D.C., 1991.

Davidson, E. A., and I. L. Ackerman, Changes in soil carbon inventories following cultivation of previously untilled soils, *Biogeochemistry*, *20*, 161-194, 1993.

Dentener, F. J., and P. J. Crutzen, Reaction of N_2O_5 on tropospheric aerosols: Impact on the global distributions of NO_x, O_3, and OH, *J. Geophys. Res.*, *98*, 7149-7163, 1993.

Dentener, F. J., and P. J. Crutzen, A three-dimensional model of the global ammonia cycle, *J. Atmos. Chem.*, *19*, 331-369, 1994.

Durka, W., E.-D. Schulze, and S. Voerkelius, Effects of forest decline on uptake and leaching of deposited nitrate determined from ^{15}N and ^{18}O measurements, *Nature*, *372*, 765-767, 1994

Edgerton, E. S., T. F. Lavery, and R. P. Boksleitner, Preliminary data from the USEPA dry deposition network: 1989, *Enviromental Pollution*, *75*(2), 145-155, 1992.

Esser, G., Modeling global terrestrial sources and sinks of CO_2 with special reference to soil organic matter, in *Soils and the Greenhouse Effect*, edited by A. F. Bouwman, pp. 247-262, John Wiley, New York, 1990.

Galloway, J. N., H. Levy II, and P. S. Kasibhatla, Year 2020: Consequences of population growth and development of deposition of oxidized nitrogen, *Ambio*, *23*(2), 120-123, 1994.

Galloway, J. N., W. H. Schlesinger, H. Levy II, A. Michaels, and J. L. Schnoor, Nitrogen fixation: Anthropogenic enhancement-environmental response, *Global Biogeochem. Cycles*, *9*, 235-252, 1995.

Hertel, O., R. Berkowicz, J. Christensen, and O. Hov, Test of two numerical schemes for use in atmospheric transport-chemistry models, *Atmos. Environ.*, *27A*, 2591-2611, 1993.

Houghton, J. T., and L. G. Meira Filho, *The IPCC Report on Radiative Forcing of Climate Change*, Cambridge Univ. Press, New York, 1994.

Hudson, R. J. M., S. A. Gherini, and R. A.Goldstein, Modeling the global carbon cycle: Nitrogen fertilization of the terrestrial biosphere and the "missing" CO_2 sink, *Global Biogeochem. Cycles*, *8*(3), 307-333, 1994.

Jacob, D. J., and P. S. Bakwin, Cycling of NO_x in tropical forest canopies, in *Microbial Production and Consumption of Greenhouse Gases: Methane, Nitrogen Oxides, and Halomethanes*, edited by J. E. Rogers and W. B. Whitman, pp. 237-254, Am. Soc. for Microbiol., Washington, D.C., 1991.

Jaeger, L., Monatskarten des Niederschlags für die ganze Erde, *Beri Dtsch. Wetterdienstes*, *139*, 1976.

Johnson, D. W., G. S. Henderson, and D. E. Todd, Changes in nutrient distribution in forests and soils of Walder Branch Watershed, Tennessee, over an eleven-year period, *Biogeochemistry*, *5*, 275-293, 1988.

Kanakidou, M., Chemistry in CTMs, Combined IGAC meeting: Global integration and modelling (GIM)/global emissions inventory activity (GEIA)/global atmospheric chemistry survey, Fairfax, Va., 1995.

Kasibhatla, P., H. Levy, A. Klonecki, and W. L. Chameides, Three-dimensional view of the large-scale tropospheric ozone distribution over the North Atlantic Ocean during summer, *J. Geophys. Res.*, *101*, 29,305-29,316, 1996.

Kasibhatla, P. S., NO_y from sub-sonic aircraft emissions: A global three-dimensional model study, *Geophys. Res. Lett.*, *20*(16), 1707-1710, 1993b.

Kasibhatla, P. S., H. Levy II, and W. J. Moxim, Global NO_x, HNO_3, PAN, and NO, distributions from fossil fuel combustion emissions: A model study, *J. Geophys. Res.*, *98*, 7165-7180, 1993a.

Kasibhatla, P. S., H. Levy II, W. J. Moxim, and W. L. Chameides, The relative impact of stratospheric photochemical production on tropospheric NO_y levels: A model study, *J. Geophys. Res.*, *96*, 18,631-18,646, 1991.

Keeling, C. D., Global historical CO_2 emissions, in *Trends '93: A Compendium of Data on Global Change*, ORNL.CDIAC:65, edited by T. A. Boden, D. P Kaiser, R. J. Sepanski, and F. W. Stoss, pp. 501-504, CDIAC, Oak Ridge Natl. Lab., Oak Ridge, Tenn., 1994.

Keeling, C. D., R. B. Bacastow, A. F. Carter, S. C. Piper, T. P. Whorf, M. Heimann, W. G. Mook, and H. Roeloffzen, A three-dimensional model of atmospheric CO_2 transport based on observed winds: 1. Analysis of observational data, in *Aspects of climate variability in the Pacific and Western Americas*, edited by D. H. Peterson, pp. 165-236, American Geophysical Union Geophysical Monograph Board, Washington, D.C., 1989.

Kohlmaier, G. H., A. Janecek, and M. Plochl, Modelling response of vegetation to both excess CO_2 and airborne nitrogen compounds within a global carbon cycle model, in *Advances in Environmental Modelling*, edited by A. Marani, pp. 207-234, Elsevier, New York, 1988.

Lamarque, J. F., G. Brasseur, P. G. Hess, and J. F. Müller, Three-dimensional study of the relative contributions of the different nitrogen sources in the troposphere, *J. Geophys. Res.*, *101*, 22,955-22,968, 1996.

Levy, H., P. S. Kasibhatla, W. J. Moxim, and J. A. Logan, The global impact of biomass burning on tropospheric reactive nitrogen, in *Proceedings Chapman Conference on Global Biomass Burning*, edited by J. Levine, pp. 263-269, MIT Press, Cambridge, Mass., 1991.

Levy, H., and W. J. Moxim, Simulated global distribution and deposition of reactive nitrogen emitted by fossil fuel combustion, *Tellus Ser. B*, *41*,256-271, 1989b.

Levy, H., W. J. Moxim, and P. S. Kasibhatla, A global three-dimensional time-dependent lightning source of tropospheric NO_x, *J. Geophys. Res.*, *101*, 22,911-22,922, 1996.

Levy, H., W. J. Moxim, and P. S. Kasibhatla, Tropospheric NO_x: Its sources and distribution, *J. Geophys. Res.*, submitted, 1996.

Likens, G. E., F. H. Bormann, and N. M. Johnson, Interactions between major biogeochemical cycles in terrestrial ecosystems, in *Some Perspectives of the Major Biogeochemical Cycles*, edited by G. E. Likens, pp. 93-112, John Wiley, New York, 1981.

Logan, J. A., Tropospheric chemistry, *J. Geophys. Res.*, *86*, 7,210-7,254, 1981.

Logan, J. A., Nitrogen oxides in the troposphere: Global and regional budgets, *J. Geophys. Res.*, *88*, 10,785-10,807, 1983.

Marland, G., R. J. Andres, and T. A. Boden, Global, regional and national CO_2 emissions, in *Trends '93: A Compendium of Data on Global Change*, ORNL.CDIAC-65, edited by T. Boden, D. P. Kaiser, R. J. Sepanski, and F. W. Stoss, pp. 505-584, CDIAC, Oak Ridge Nat. Lab., Oak Ridge, Tenn., 1994.

Matson, P. A., T. Billow, J. Panek, I. Ortiz Monasterio, and R. Naylor, Fertilizer management and consequences for nitrogen trace gases emissions from Mexican wheat systems, Ecol. Soc. of Am., Providence, R.I., 1996.

Matthews, E., Global vegetation and land use: New high-resolution data bases for climate studies, *J. Climate Appl. Meteorol.*, *22*, 474-487, 1983.

McLaughlin, S. B., and D. J. Downing, Interactive effects of ambient ozone and climate measured on growth of mature forest trees, *Nature*, *374*, 252-254, 1995.

McNulty, S. G., and J. D. Aber, Effects of chronic nitrogen additions on nitrogen cycling in a high-elevation spruce-fir stand, *Can. J. For. Res.*, *23*, 1252-1263, 1993.

Moxim, W. J., H. Levy, and P. S. Kasibhatla, Simulated global tropospheric PAN: Its transport and impact on NO_x, *J. Geophys. Res.*, *101*, 12,621-12,638, 1996.

Müller, J. F., Geographical distribution and seasonal variation of surface emissions and deposition velocities of atmospheric trace gases, *J. Geophys. Res.*, *97*, 3787-3804, 1992.

Müller, J. F., and G. Brasseur, IMAGES: A three-dimensional chemical transport model of the global troposphere, *J. Geophys. Res.*, *100*, 16,445-16,490, 1995.

National Atmospheric Deposition Program (NRSP-3)/National Trends Network, NADP/NTN Coordination Office, Natural Resource Ecology Laboratory, Colorado State University, Fort Collins, Colo., 1995.

Nevison, C. D., G. Esser, and E. A. Holland, A global model of changing N_2O emissions from natural and perturbed soils, *Clim. Change*, *32*, 327-378, 1996.

Newell, R. E., J. W. Kidson, D. G. Vincent, and G. J. Boer, *The General Circulation of the Tropical Atmosphere and Interactions with Extra Tropical Latitudes*, vol. 2, MIT Press, Cambridge, Mass., 1974.

Oort, A. H., Global atmospheric circulation statistics, 1958-1973, Natl. Oceanic and Atmos. Admin., NOAA Prof. Pap., report number 14, 1983.

Parton, W. J., D. S. Schimel, C. V. Cole, and D. S. Ojima, Analysis of factors controlling soil organic matter levels in Great Plains grasslands, *Soil Sci. Soc. Am. J.*, *51*, 1173-1179, 1987.

Parton, W. J., J. M. O. Scurlock, and D. S. Ojima, Observations and modeling of biomass and soil organic matter dynamics for the grassland biome worldwide, *Global Biogeochem. Cycles*, *7*(4), 785-809, 1993.

Penner, J. E., C. S. Atherton, J. Dignon, S. J. Ghan, and J. J. Walton, Tropospheric nitrogen: A three dimensional study of sources, distributions, and deposition, *J. Geophys. Res.*, *96*, 959-990, 1991.

Penner, J. E., C. S. Atherton, and T. E. Graedel, Global emissions and models of photochemically active compounds, in *Global Atmospheric-Biospheric Chemistry*, edited by R. G. Prinn, pp. 223-247, Plenum, New York, 1994.

Peterson, B. J., and J. M. Melillo, The potential storage of carbon caused by eutrophication of the biosphere, *Tellus Ser. B*, *37*, 117-127, 1985.

Prather, M., R. Derwent, D. Ehhalt, P. Fraser, E. Sanhueza, and X. Zhou, Other trace gases and atmospheric chemistry, in *Climate Change 1994: Radiative Forcing of Climate Change and An Evaluation of the IPCC IS92 Emission Scenarios*, edited by J. T. Houghton, et al., pp. 75-126, Cambridge Univ. Press, New York, 1995.

Reich, P. B., Quantifying plant response to ozone: A unifying theory, *Tree Physiol.*, *3*, 63-91, 1987.

Roelofs, G.-J., and J. Lelieveld, Distribution and budget of O_3 in the troposphere calculated with a chemistry-general circulation model, *J. Geophys. Res.*, *100*, 20,983-20,988, 1995.

Schimel, D., I. G. Enting, M. Heimann, T. M. L. Wigley, D. Raynaud, D. Alves, and U. Siegenthaler, CO_2 and the carbon cycle, in *Climate Change 1994: Radiative Forcing of Climate Change and an Evaluation of the IPCC IS92 Emission Scenarios*, edited by J. T. Houghton, et al., pp. 35-71, Cambridge Univ. Press, New York, 1995.

Schimel, D. S., Terrestrial ecosystems and the carbon cycle, *Global Change Biol.*, *1*, 77-91, 1995.

Schimel, D. S., Climate and nitrogen controls on the geography and timescales of terrestrial biogeochemical cycling, *Global Biogeochem. Cycles*, *10*, 677-709, 1996.

Schimel, D. S., J. B. H. Braswell, E. A. Holland, R. McKeown, D. S. Ojima, T. H. Painter, W. J. Parton, and A. R. Townsend, Climatic, edaphic, and biotic controls over carbon and turnover of carbon in soils, *Global Biogeochem. Cycles*, *8*, 279-293, 1994.

Schindler, D. W., and S. E. Bayley, The biosphere as an increasing sink for atmospheric carbon: Estimates from increased nitrogen deposition, *Global Biogeochem. Cycles*, *7*, 717-733, 1993.

Schlesinger, W. H., *Biogeochemistry: An Analysis of Global Change*, Academic Press, San Diego, Calif., 1991.

Schlesinger, W. H., and A. E. Hartley, A global budget for atmospheric NH_3, *Biogeochemistry*, *15*, 191-211, 1992.

Schulze, E.-D., Air pollution and forest decline in a spruce (*Picea abies*) forest, *Science*, *244*, 776-783, 1989.

Shea, D. J., Climatological Atlas: 1950-1979, Natl. Ctr. Atmos. Res., NCAR Tech. Note, *NCAR/TN-269+STR*, 1986.

Shepherd, M. F., S. Barzetti, and D. R. Hastie, The production of atmospheric NO_x and N_2O from a fertilized agricultural soil, *Atmos. Environ.*, *25*, 1961-1969, 1991.

Tans, P. P., I. Y. Fung, and I. G. Enting, Storage versus flux budgets: The terrestrial uptake of CO_2 during the 1980's, in *Biotic Feedbacks in the Global Climate System: Will the Warming Feed the Warming*, edited by G. M. Woodwell and F. T. Mackenzie, Oxford Univ. Press, New York, 1994.

Townsend, A. R., B. H. Braswell, E. A. Holland, and J. E. Penner, Spatial and temporal patterns in potential terrestrial carbon storage resulting from deposition of fossil fuel derived nitrogen, *Ecol. Appl.*, *6*(3), 806-814, 1996.

Trenberth, D. E., and J. G. Olson, Intercomparisons of NMC and ECMWF global, Natl. Ctr. Atmos. Res., NCAR Tech. Note, *NCAR/TN-229+STR*, 1988a.

Trenberth, D. E., and J. G. Olson, ECMWF global Analyses 1979-1986: Circulation statistics and data evaluation, Natl. Ctr. Atmos. Res., NCAR Tech. Note, *NCAR/TN-300+STR*, 1988b.

Vitousek, P. M., Beyond global warming: Ecology and global change, *Ecology*, *75*, 1861-1876, 1994.

Yienger, J. J., and H. Levy II, An empirical model of global soil-biogenic NO_x emissions, *J. Geophys. Res.*, *100*, 11,447-11,464, 1995.

Zimmermann, P. H., MOGUNTIA: A handy global tracer model, Proceedings of the Sixteenth NATO/CCMS International Technical Meeting on Air Pollution Modeling and Its Application, New York, 1988.

Zimmermann, P. H., J. Feichter, H. K. Rath, P. J. Crutzen, and W. Weiss, A global three-dimensional source-receptor model investigation using ^{85}Kr, *Atmos. Environ.*, *23*, 25-35, 1989.

G. Brasseur, E. A. Holland, J.-F. Lamarque, J. Sulzman, and A. Townsend, National Center for Atmospheric Research, Boulder, CO 80307-3000. (e-mail: eholland@ncar.ucar.edu)

B. H. Braswell, University of New Hampshire, Durham, NH 03824.

F. Dentener, Department of Air Quality, Wageningen Agricultural University, DNL 6700 EV Wageningen, The Netherlands.

H. Levy II, Geophysical Fluid Dynamics Laboratory, Princeton, NJ 08542.

J.-F. Müller, Belgian Institute for Space Aeronomy, B-1180 Brussels, Belgium.

J. E. Penner, Atmospheric Oceanic, and Space Sciences, University of Michigan, 2455 Hayward, Ann Arbor, MI 48109-2143.

G.-J. Roelofs, Institute for Marine and Atmospheric Research Utrecht (IMAU), Princeontplein 53584 CC Utrecht, The Netherlands.

(Received May 2, 1996; revised September 20, 1996; accepted October 3, 1996.)